

Learning Dynamics of LLM Finetuning

Yi Ren^{*1} and Danica J. Sutherland^{†1,2}

¹Department of Computer Science, University of British Columbia

²Alberta Machine Intelligence Institute

July 2024

Abstract

Learning dynamics, which describes how the learning of specific training examples influences the model’s prediction of other examples, give us a powerful tool for understanding the behavior of deep learning systems. We study the learning dynamics of large language models during finetuning, by analyzing the step-wise decomposition and accumulated influence among different responses. Our framework allows a uniform interpretation of many interesting observations about the training of popular algorithms for both instruction tuning and preference tuning. The analysis not only explains where the benefits of these methods come from but also inspires a simple, effective method to further improve the alignment performance. Code for experiments is available at https://github.com/Joshua-Ren/Learning_dynamics_LLM.

1 Introduction

Deep neural networks usually acquire new knowledge by updating their parameters via gradient descent (GD). This procedure can be described by learning dynamics, which links changes in the model’s predictions to the gradients generated by learning from specific examples. With the help of learning dynamics, researchers have not only explained many interesting phenomena during training, but used these insights to propose novel, improved algorithms (Pruthi et al. 2020; Ren, Guo, et al. 2023; Xia et al. 2024).

The study of large language models (LLM) is gaining popularity due to their surprising capabilities on various tasks. To ensure the LLMs follow human instructions and align well with human values, finetuning has attracted much recent attention. Practitioners often start with instruction tuning, where the model learns extra knowledge necessary for the downstream task (such as instruction-following), and then preference tuning, where the model aligns its outputs to human preference (Ouyang et al. 2022). Various finetuning algorithms have been proposed to fit into this pipeline, with differing explanations as to why they improve the model’s performance.

Different from most existing analyses of LLM finetuning, which use the perspective of their training targets, their status at the end of training, or their relationships to reinforcement learning (e.g. Ji et al. 2024; Rafailov et al. 2024; Tajwar et al. 2024), this paper tries to understand LLMs’ evolution from a dynamical perspective. Specifically, we formalize the learning dynamics of LLMs’ finetuning using a similar decomposition of gradient updates to that of Ren et al. (2022). Surprisingly, this framework can be easily adapted to various finetuning algorithms with different goals, including supervised finetuning (SFT, Wei et al. 2022), self-play finetuning (SPIN, Z. Chen et al. 2024), direct preference optimization (DPO, Rafailov et al. 2023), and their variants. This framework has the potential to explain several interesting and counter-intuitive observations during training – including the “repeater” phenomenon after preference tuning (Holtzman et al. 2020), hallucination¹ (Huang et al. 2023), the decay in confidence of *all* responses during off-policy DPO (Rafailov et al. 2024), and more.

Moreover, we also provide a new perspective on understanding why off-policy DPO and other variants underperform their on-policy counterpart (Guo, B. Zhang, et al. 2024). Our explanation starts by observing an interesting “squeezing effect,” which we demonstrate is a consequence of gradient *ascent* (as in DPO and similar algorithms) on models with cross-entropy loss following a softmax layer. In short, for each token’s prediction, the negative gradient will push down the model’s predictions on (almost) all possible output labels, moving this

^{*}renyi.joshua@gmail.com [†]dsuth@cs.ubc.ca

¹Especially the case that the model uses facts or phrases that appear in the responses of question B to answer question A.

probability mass to the most-likely labels. This can be detrimental to the alignment we are trying to achieve. This effect is most serious when the negative gradient is imposed on an already-unlikely label, which is why the confidence of almost all responses decreases during off-policy DPO. Inspired by our analysis, we propose a simple, counter-intuitive, but very effective method to further improve alignment performance.

2 Background and Related Works

2.1 Learning dynamics of deep learning

When studying a practical machine learning algorithm, we usually care about how the learned model f_θ is influenced by different factors, e.g., the model’s parameter θ , the training dataset, the learning hyperparameters, etc. Broadly speaking, “learning dynamics” is usually used as an umbrella term to describe how the change of a specific factor influences the model’s prediction. In this paper, we narrow down this term to describe “how the change in θ influences the corresponding change in f_θ ”, i.e., the relationship between $\Delta\theta$ and Δf_θ .

For a simple model like $f_{a,b}(x) = ax^2 + b$, it is straightforward to directly manipulate $\Delta\theta$ and observe the resulting Δf_θ accordingly. However, for a deep neural network, such an observation is impractical for many reasons. First, a deep model usually contains an enormous number of parameters, individual parameters are usually very difficult to interpret. Second, the input and output spaces of the model $f_\theta(x)$ are usually high-dimensional, making it hard to observe Δf_θ directly. Combining the fact that modern deep models are usually trained via different variants of stochastic gradient descent (SGD), where all parameters change simultaneously in each update, we usually use the following definition to study learning dynamics:

$$\Delta\theta \triangleq \theta^{t+1} - \theta^t = -\eta \cdot \nabla\mathcal{L}(f_\theta(\mathbf{x}_u)); \quad \Delta f(\mathbf{x}_o) \triangleq f_{\theta^{t+1}}(\mathbf{x}_o) - f_{\theta^t}(\mathbf{x}_o). \quad (1)$$

Here the update of θ during step $t \rightarrow t + 1$ is given by learning the sample \mathbf{x}_u using SGD with learning rate η . In short, the learning dynamics in this paper address the question:

After an SGD update on \mathbf{x}_u , how does the model’s prediction on \mathbf{x}_o change?

Studying the learning dynamics defined above can shed light on many important problems in deep learning and also help to understand various counter-intuitive phenomena. Here are a few.

Understanding generalization. If we consider \mathbf{x}_u from the training set, and \mathbf{x}_o from the test set, this form of learning dynamics addresses generalization: the model generalizes better if the loss of $f_\theta(\mathbf{x}_o)$ keeps decreasing when it learns from \mathbf{x}_u . By studying the influence of different \mathbf{x}_u at different stages during supervised learning, Ren et al. (2022) explain a “zigzag” pattern of the learning path, which sheds light on why the model can spontaneously pursue better supervisory signals and correct noisy labels in the early stage of training (see also S. Liu et al. 2020). Kumar et al. (2022) and Ren, Guo, et al. (2023) apply learning dynamics to explain why directly finetuning a well-trained backbone with a randomly initialized task head might harm the out-of-distribution generalization ability. Ren et al. (2020) and Ren, Lavoie, et al. (2023) also explains where the simplicity bias favoring compositional representations comes from during knowledge distillation (Hinton et al. 2015), providing a new perspective of understanding why successive knowledge transferring can improve the model’s systematic generalization ability.

Measuring the “quality” or “influence” of training samples. Besides explaining the model’s behavior, learning dynamics is also helpful for evaluating the quality or the effectiveness of different training samples. For example, Pruthi et al. (2020) propose a quantitative metric called **TracIn** to compute the influence of a training example on the predictions made by the model. This metric is then applied by Xia et al. (2024) to search for the most influential examples in LLM instruction finetuning. By expanding Equation (1) in the neural tangent kernel (NTK) regime, Guo, Ren, et al. (2024) propose a metric called **1pNTK** to measure the relative difficulty among different training samples. These metrics and analyses inspired by learning dynamics are expected to be helpful in many related fields, like coreset selection (Feldman 2020), active learning (Settles 2009) (see, e.g., Mohamadi et al. 2022), and dataset distillation (T. Wang et al. 2018).

2.2 Challenges of Analyzing the Learning Dynamics of LLM’s Finetuning

The first conundrum for analyzing the learning dynamics of LLM’s finetuning is the high dimensionality and the sequence nature of *both* the input and output signals. The high-dimensional property makes it hard to observe the model’s output, and the sequence nature makes the distributions on different tokens mutually dependent,

which is more complicated than a standard multi-label classification problem considered by most previous works. Furthermore, as there are many different algorithms for LLM finetuning – SFT (Wei et al. 2022), RLHF (Ouyang et al. 2022), DPO (Rafailov et al. 2023), etc. – analyzing them under a uniform framework is challenging. Finally, compared with the training-from-scratch scenario, where a roughly uniform distribution over all possible outputs is usually assumed at the beginning of training, LLMs’ finetuning dynamics heavily rely on the pretrained base model, which could make the analysis harder. For example, the pretrained model usually assigns little probability mass to unlikely tokens, which is good for most practical applications but leads to risk of the “squeezing effect” we show later.

In the remainder of the paper, we will tackle the aforementioned problems and propose a unified framework to describe different finetuning algorithms. We believe studying the learning dynamics provides a complementary perspective on LLM finetuning behaviors to the usual analyses of where different algorithms eventually converge.

3 Learning Dynamics under Per-step and Accumulated Perspectives

We first consider a standard supervised learning problem, where the model takes a high-dimensional input \mathbf{x} and generates a sequence response $\mathbf{y} = \{y_1, \dots, y_L\} \in \mathcal{V}^L$, where \mathcal{V} is the vocabulary of size V . We assume we actually define a distribution over \mathbf{y} , i.e., $\pi_\theta(\mathbf{y} | \mathbf{x})$. To get this probabilistic distribution, the model first generates a logits matrix $\mathbf{z} = h_\theta(\mathbf{x}) \in \mathbb{R}^{V \times L}$ and then takes the Softmax operation on each column. To make the analysis for the LLM case easier, we track the change of $\log \pi_{\theta^t}$ instead of π_{θ^t} , slightly different from the results of Ren et al. (2022).

Per-step influence decomposition. The learning dynamics of (1) become

$$\Delta\theta \triangleq \theta^{t+1} - \theta^t = -\eta \cdot \nabla \mathcal{L}(\pi_\theta(\mathbf{y} | \mathbf{x}_u), \mathbf{y}_u) \quad (2)$$

$$\Delta \log \pi^t(\mathbf{y} | \mathbf{x}_o) \triangleq \log \pi_{\theta^{t+1}}(\mathbf{y} | \mathbf{x}_o) - \log \pi_{\theta^t}(\mathbf{y} | \mathbf{x}_o), \quad (3)$$

where $\mathbf{y}_u \in \mathbb{R}^V$ (likely one-hot) is the supervisory signal. To get a better intuition, we start from the $L = 1$ scenario, where the $\Delta\theta$ and $\Delta\pi$ can be linked by the following proposition.

Proposition 1 (Similar to Proposition 1 of Ren et al. 2022). *Let $\pi = \text{Softmax}(\mathbf{z})$ and $\mathbf{z} = h_\theta(\mathbf{x})$. The one-step learning dynamics decompose as*

$$\underbrace{\Delta \log \pi^t(\mathbf{y} | \mathbf{x}_o)}_{V \times 1} = -\eta \underbrace{\mathcal{A}^t(\mathbf{x}_o)}_{V \times V} \underbrace{\mathcal{K}^t(\mathbf{x}_o, \mathbf{x}_u)}_{V \times V} \underbrace{\mathcal{G}^t(\mathbf{x}_u, \mathbf{y}_u)}_{V \times 1} + O(\eta^2 \|\nabla_\theta \mathbf{z}(\mathbf{x}_u)\|_{\text{op}}^2), \quad (4)$$

where $\mathcal{A}^t(\mathbf{x}_o) = \nabla_{\mathbf{z}} \log \pi_{\theta^t}(\mathbf{x}_o) = I - \mathbf{1}\pi_{\theta^t}^\top(\mathbf{x}_o)$, $\mathcal{K}^t(\mathbf{x}_o, \mathbf{x}_u) = (\nabla_\theta \mathbf{z}(\mathbf{x}_o)|_{\theta^t})(\nabla_\theta \mathbf{z}(\mathbf{x}_u)|_{\theta^t})^\top$ is the empirical neural tangent kernel of the logit network and $\mathcal{G}^t(\mathbf{x}_u, \mathbf{y}_u) = \nabla_{\mathbf{z}} \mathcal{L}(\mathbf{x}_u, \mathbf{y}_u)|_{\mathbf{z}^t}$, which for cross-entropy loss is $\pi_{\theta^t}(\mathbf{y} | \mathbf{x}_u) - \mathbf{y}_u$.

The proof and more discussion can be found in Appendix A.

In this decomposition, $\mathcal{A}^t(\mathbf{x}_o) = I - \mathbf{1}\pi_{\theta^t}^\top(\mathbf{x}_o)$, which only depends on the model’s predicted probability at time t . Intuitively, for any length- V vector \mathbf{b} , left-multiplying this $V \times V$ matrix \mathcal{A}^t centers the vector with respect to the probability distribution $\pi_{\theta^t}(\mathbf{x}_o)$, because $\mathcal{A}^t \mathbf{b} = (I - \mathbf{1}\pi^\top) \mathbf{b} = \mathbf{b} - \mathbf{1}(\pi^\top \mathbf{b})$, and hence the mean of $\mathcal{A}^t \mathbf{b}$ under π is $\pi^\top \mathbf{b} = 0$.

The matrix \mathcal{K}^t is the empirical neural tangent kernel (eNTK, Jacot et al. 2018; J. Lee et al. 2019) of the model, i.e., the product of the model’s gradients with respect to \mathbf{x}_o and \mathbf{x}_u . Since the eNTK usually changes slowly (or is even nearly invariant) when finetuning with a small learning rate (Jacot et al. 2018; Arora et al. 2019; Fort et al. 2020; Ren, Guo, et al. 2023), we can treat \mathcal{K}^t as a relatively stable and model-specific similarity measurement between different input samples: larger $\|\mathcal{K}^t\|$ means the update of \mathbf{x}_u can influence model’s prediction on \mathbf{x}_o more. The term \mathcal{G}^t is determined by the loss function \mathcal{L} , which usually provides the *energy* and *direction* for the model’s adaptation. For example, consider a cross-entropy loss $\mathcal{L}_{\text{CE}} \triangleq -\mathbf{y}_u \cdot \log \pi(\mathbf{y} | \mathbf{x}_u)$. Then we have $\mathcal{G}_{\text{CE}}^t = \pi_{\theta^t}(\mathbf{y} | \mathbf{x}_u) - \mathbf{y}_u$, a length- V vector that points from the model’s current predictive distribution to the desired supervisory distribution. When considering one-hot labels, the above term can also be written as $\mathcal{G}_{\text{CE}}^t = \pi_{\theta^t}(\mathbf{y} | \mathbf{x}_u) - \mathbf{e}_{y_u}$, which is more common in practice.

For a multi-label classification problem where $L > 1$, to this first-order approximation, we only need to calculate L different $\Delta \log \pi^t$ and stack them together.

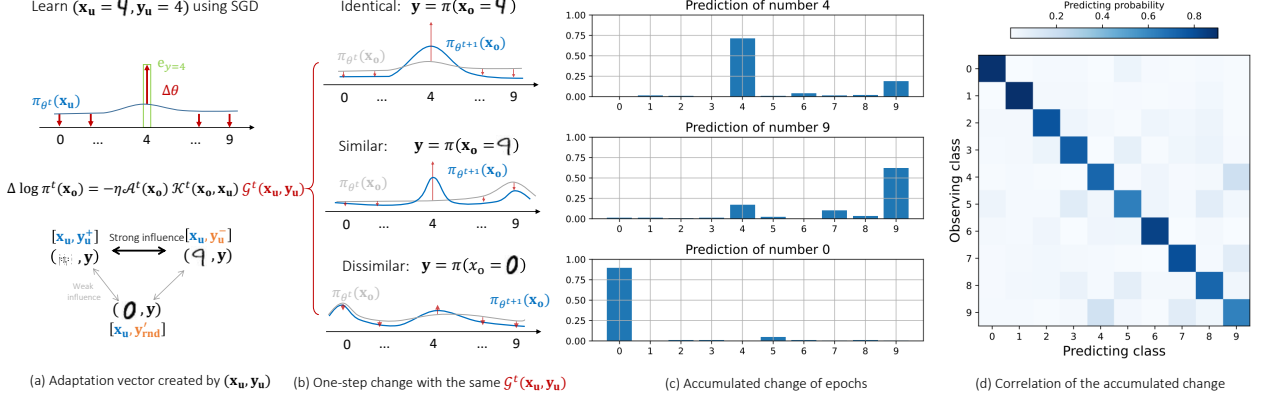


Figure 1: The per-step learning dynamics and the accumulated influence in an MNIST experiment.

Accumulated influence: a simple example on MNIST.

Proposition 1, which states how the update of \mathbf{x}_u changes the model’s prediction on \mathbf{x}_o , provides us with a powerful tool for understanding the mutual influence between the update of different samples during training.

As a warm-up, we first analyze an example of training a LeNet on the MNIST dataset (LeCun et al. 1998). See Figure 1-(a), where the network π_{θ^t} is updating its parameters using the loss calculated on one training example $(\mathbf{x}_u, \mathbf{y}_u = \mathbf{e}_4)$, where \mathbf{e}_4 is the one-hot vector corresponding to a label of class 4. The residual term $\mathcal{G}_{\text{CE}}^t(\mathbf{x}_u, \mathbf{y}_u)$ is then represented by the red arrows, which all start from $\pi_{\theta^t}(\mathbf{y} | \mathbf{x}_u)$ and point to \mathbf{y}_u . We can then ask how the model’s prediction on different \mathbf{x}_o changes after this update. As illustrated in Figure 1-(b), for an \mathbf{x}_o in the same class with \mathbf{x}_u (i.e., the identical case), the predicted probability of this correct label is “pulled up” by this update, as expected. Supposing this \mathbf{x}_o is from the test set, this update makes the model more confident in correctly predicting an unseen sample. On the other hand, if this \mathbf{x}_o is similar to \mathbf{x}_u (i.e., $\|\mathcal{K}^t\|$ is reasonably large) but comes from another class, then the predicted probability on \mathbf{x}_u ’s class (which is not the correct label of \mathbf{x}_o) would be “pulled up.” Last, for examples that look dissimilar to \mathbf{x}_u ($\|\mathcal{K}^t\|$ is small), this update will not change the model’s prediction on \mathbf{x}_o much, as illustrated in the bottom panel in Figure 1-(b).

The interactions among the updates of different inputs then form an interesting pattern for the learned predictions. As illustrated in Figure 1-(c), when making predictions on images coming from class 4, the model tends to assign higher confidence on class 9. That is because the examples in class 9 on average look more similar to class 4 than examples in other classes. Hence the update of examples in classes 4 and 9 will reinforce their mutual influence and lead to a bump in their predictions. To further verify this, we plot the average value of $\pi(\mathbf{y} | \mathbf{x})$ for \mathbf{x} from each of the classes in Figure 1-(d). In this heatmap, the indexes of the rows denote which class the images come from. The values of some off-diagonal patches are significantly higher than others, which means the examples in the corresponding classes look more similar, like 4 and 9, 5 and 3, 8 and 5, etc.

4 Learning Dynamics of LLM Supervised Finetuning

Per-step decomposition of the SFT loss.

We are now ready to tackle the supervised finetuning (SFT) of an LLM. The typical loss function used in this stage is the negative log-likelihood (NLL) of a given completion $\mathbf{y}_u^+ = (y_1^+, \dots, y_L^+) \in \mathcal{V}^L$, conditioned on the prompt \mathbf{x}_u :

$$\mathcal{L}_{\text{SFT}}(\mathbf{x}_u, \mathbf{y}_u^+) \triangleq - \sum_{l=1}^L \log \pi(y = y_l^+ | \mathbf{y}_{1:l-1}^+, \mathbf{x}_u) = - \sum_{l=1}^L \mathbf{y}_l^+ \cdot \log \pi(\mathbf{y} | \mathbf{x}_u, \mathbf{y}_{1:l-1}^+). \quad (5)$$

Note that compared with the multi-label classification problem discussed before, where the joint distribution of all labels can be factorized as $\pi(\mathbf{y} | \mathbf{x}) = \prod_l \pi(y_l | \mathbf{x})$, the sequential nature of language modeling makes the analysis more complicated, because we must have $\pi(\mathbf{y} | \mathbf{x}) = \prod_l \pi(y_l | \mathbf{x}, \mathbf{y}_{1:l-1})$. Note that this is the correct form, and not one conditioning on the previous model predictions, due to the “teacher forcing” scheme typically used in training sequence models. To solve this problem, we can merge this factorization into the definition of the backbone h_θ while keeping the decomposition format of Proposition 1. Specifically, define $\chi \triangleq [\mathbf{x}; \mathbf{y}]$. Then

for the prediction of all tokens of \mathbf{y} , we have

$$\mathbf{z} = h_\theta(\boldsymbol{\chi}); \quad \pi(\mathbf{y} | \boldsymbol{\chi}) = \text{Softmax_column}(\mathbf{z}).$$

Note that \mathbf{z} is a $V \times L$ matrix where each column contains the logits of the prediction of the l -th token. Our h_θ , even taking the entire sequence $\boldsymbol{\chi}$ as its input, will force the model not to refer to the future tokens $\mathbf{y}_{>l}$ when making predictions on the l -th token, which is commonly implemented via ‘‘causal masking’’ (e.g. Vaswani et al. 2017). Then, we can calculate $(\nabla_{\theta} \mathbf{z}_l(\boldsymbol{\chi}_o)|_{\theta^t})(\nabla_{\theta} \mathbf{z}_l(\boldsymbol{\chi}_u)|_{\theta^t})^\top$ on each column of \mathbf{z} and then stack them to form a $V \times V \times L$ tensor $\mathcal{K}^t(\boldsymbol{\chi}_o, \boldsymbol{\chi}_u)$. The calculation of \mathcal{G}^t and \mathcal{A}^t also follows a similar procedure. Thanks to the causal mask implemented in h_θ , the resulting decomposition is almost identical to that in a multi-label classification problem.

Assume now we have a response \mathbf{y}_u of length L associated with \mathbf{x}_u , stacked into $\boldsymbol{\chi}_u$, and \mathbf{y}_o of length M associated with \mathbf{x}_o , stacked into $\boldsymbol{\chi}_o$. The change of the model’s prediction on the m -th token of \mathbf{y}_o can be represented as

$$\underbrace{[\Delta \log \pi^t(\mathbf{y} | \boldsymbol{\chi}_o)]_m}_{V \times M} = - \sum_{l=1}^L \eta \underbrace{[\mathcal{A}^t(\boldsymbol{\chi}_o)]_m}_{V \times V \times M} \underbrace{[\mathcal{K}^t(\boldsymbol{\chi}_o, \boldsymbol{\chi}_u)]_l}_{V \times V \times L} \underbrace{[\mathcal{G}^t(\boldsymbol{\chi}_u)]_l}_{V \times L} + O(\eta^2) \quad (6)$$

Compared with Proposition 1, the main difference is that the eNTK term also depends on the responses \mathbf{y}_u and \mathbf{y}_o , which allows us to answer questions like ‘‘how learning $(\mathbf{x}_u, \mathbf{y}_u^+)$ influences the model’s belief about $(\mathbf{x}_u, \mathbf{y}_u^-)$ ’’. Combined with the SFT loss, the residual term is

$$\mathcal{G}_{\text{SFT}}^t(\boldsymbol{\chi}_u) = \nabla_{\mathbf{z}} \mathcal{L}_{\text{SFT}}(\boldsymbol{\chi}_u)|_{\mathbf{z}^t} = \underbrace{\pi_{\theta^t}(\mathbf{y} | \boldsymbol{\chi}_u)}_{V \times L} - \underbrace{\mathbf{y}_u}_{V \times L}, \quad (7)$$

almost identical to that of a multi-label classification problem.

4.1 Response Space and the Probing Dataset

Besides the sequential nature of the loss function, another conundrum in analyzing LLM learning dynamics is the huge response space \mathcal{Y} : the number of possible $\mathbf{y} \in \mathcal{Y}$ is V^L , but the vast majority of possible sequences look nothing like natural language, and we expect the model to generate only a subset of natural language-like responses. These properties prevent us from observing the changes of all possible \mathbf{y} like what we did for MNIST. Instead, we define several interesting regions of \mathcal{Y} , and select corresponding typical responses to observe. Intuitively, we can use the semantic relevance between \mathbf{y} and \mathbf{x}_u as a heuristic. Such a measurement can be understood as ‘‘how suitable this \mathbf{y} is as a response to \mathbf{x}_u , compared to \mathbf{y}_u^+ .’’ Then, starting from the structure of common preference optimization datasets such as **Antropic-HH** (Y. Bai et al. 2022) and **UltraFeedback** (Cui et al. 2023), we can roughly divide \mathcal{Y} into three sub-spaces and propose seven typical responses to evaluate (as in Figure 2):

- \mathcal{Y}_{IF} : reasonable responses following the instruction \mathbf{x}_u :
 1. \mathbf{y}_u^+ , the chosen (i.e., the preferred) response to \mathbf{x}_u .
 2. \mathbf{y}_u^- , the rejected (i.e., the less preferred, but still reasonable) response to \mathbf{x}_u .
- $\mathcal{Y}_{\text{non-IF}}$: irrelevant responses to \mathbf{x}_u that are still recognizably human language (in these datasets, roughly ‘‘internet-standard’’ English):
 3. $\mathbf{y}_{j \neq u}^+$, the chosen response for a different question $\mathbf{x}_{j \neq u}$ selected from the training set.
 4. $\mathbf{y}_{\text{test}}^+$, the chosen response of a question \mathbf{x}_{test} selected from the test set.
 5. \mathbf{y}_{hum} , a ‘‘random’’ English sentence generated by GPT4 with as many words as \mathbf{y}_u^+ .
- $\mathcal{Y}_{\text{non-hum}}$: token sequences that do not form meaningful human language:
 6. $\mathbf{y}_{\text{urnd}}^+$, a random permutation of the words (space-separated strings) of \mathbf{y}_u^+ .
 7. \mathbf{y}'_{rnd} , a random permutation of the words of a generated sentence as in \mathbf{y}_{hum} .

In Appendix B.1, we also consider the Levenshtein (edit) distance to \mathbf{y}_u^+ as another axis, and track more responses accordingly. As shown by Xia et al. (2024), the influence between samples (roughly speaking, $\|\mathcal{K}^t\|$) is better captured by semantic similarity than the superficial edit distance, so we do not consider this metric in most of our results.

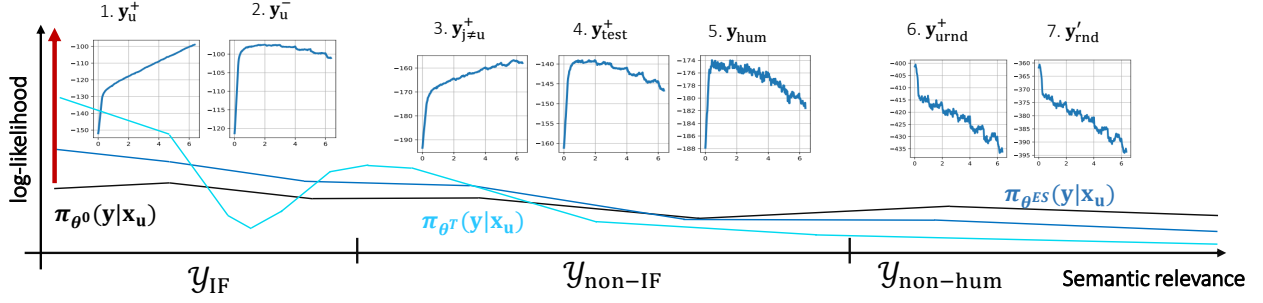


Figure 2: The division of \mathcal{Y} and seven typical selected responses. The small panels demonstrate how the average predicted probability of specific responses evolves during SFT. The three curves with different colors roughly represent the model’s prediction of the three stages of finetuning: before SFT (π_{θ^0}), early stopping after training a few epochs ($\pi_{\theta^{ES}}$), and the overfitted case (π_{θ^T}).

4.2 Experimental verification

We now verify our analysis of the learning dynamics using experiments. We first create an SFT training set by randomly selecting 5000 examples from the training split of **Antropic-HH**; we give similar results for **UltraFeedback** in Appendix B.2. The model will be finetuned using these $[\mathbf{x}; \mathbf{y}^+] \in \mathcal{D}_{\text{train}}$ for several epochs. To observe the learning dynamics, we create a probing dataset by first selecting 500 prompts from $\mathcal{D}_{\text{train}}$ and then generate seven different responses for each \mathbf{x} following Figure 2. We evaluate the log-likelihood of these responses every 25 updates (with a training batch size of 4, the probing occurs every 100 examples). The model is finetuned for 8 epochs, where we call the first several epochs from π_{θ^0} to $\pi_{\theta^{ES}}$ *fitting stage* and the last several epochs from $\pi_{\theta^{ES}}$ to π_{θ^T} *overfitting stage*. We verify the generalizability of our findings by using six models: **pythia-410M/1B/1.4B/2.8B** (Biderman et al. 2023) and **Qwen1.5-0.5B/1.8B** (J. Bai et al. 2023).

We emphasize beforehand that while the behaviors seen in this section are perhaps not particularly surprising, they validate that our learning dynamics explanations can explain practical behavior in LLM finetuning, and that these techniques *will* yield a surprising “squeezing” effect when applying them to preference finetuning in the next section.

Behaviors of $\mathbf{y} \in \mathcal{Y}_{\text{IF}}$. As illustrated in the first panel in Figure 3, in the fitting stage, we see SFT “pulls up” the curve of this region. That is because their $\mathcal{K}^t([\mathbf{x}_u, \mathbf{y}], [\mathbf{x}_u, \mathbf{y}_u^+])$ are usually large enough, which is similar to the pairing effect of 4 and 9 in the MNIST experiment. As the training goes on, the model enters into the overfitting stage, where $\pi_{\theta^t}(\mathbf{y}_u^-)$ starts to plateau and then decrease while $\pi_{\theta^t}(\mathbf{y}_u^+)$ keeps increasing. That is because the energy provided by residual term $\mathcal{G}_{\text{SFT}}^t$ always points to \mathbf{y}_u^+ while deviating from other \mathbf{y} . As the training goes on and the energy in the main direction decreases (because the model’s confidence in the target increases, which makes the gap between the current prediction and the one-hot supervisions becomes smaller), the deviating energy will gradually dominate and “push down” those regions.

Behaviors of $\mathbf{y} \in \mathcal{Y}_{\text{non-hum}}$. The learning dynamics for this region is simpler: the predictions start from a very low log-likelihood and keep decreasing throughout training, as illustrated in the last two panels in Figure 2 and the second panel in Figure 3. The responses in this region play a similar role to the 0 examples in the MNIST experiment: as they usually look dissimilar to 4, hence the norms of the corresponding \mathcal{K}^t are small, which leads to only tiny pressure “upwards” when the model learns. On the other hand, as the responses of all possible \mathbf{y} given \mathbf{x}_u must sum to one, increasing of $\pi_{\theta^t}(\mathbf{y})$ on other groups must naturally “push down” the curve in this region. Another interesting finding is that $\pi_{\theta^t}(\mathbf{y}'_{\text{rnd}})$ is always bigger than $\pi_{\theta^t}(\mathbf{y}_{\text{urnd}}^+)$, where the latter contains all the words from \mathbf{y}_u^+ . That is because learning the chosen response increases the likelihood of specific phrases, e.g., $[y_1, y_2]$. Then, in $\pi_{\theta^t}(\mathbf{y}_{\text{urnd}}^+)$, if y_1 is followed by $y_3 \neq y_2$, the resulting prediction would be very small.

Behaviors of $\mathbf{y} \in \mathcal{Y}_{\text{non-IF}}$. This group is the most complex one because first, we must consider the influence coming from the update of another training example, e.g., $[\mathbf{x}_{j \neq u}; \mathbf{y}_{j \neq u}^+]$. Furthermore, although the responses in this group are irrelevant to \mathbf{x}_u , they are reasonable human language and the model will assign non-negligible probability mass to them. That means if we want to sample a response from the model given \mathbf{x}_u (e.g., when deploying the model or doing on-policy training), the probability that the model provides a response from (or

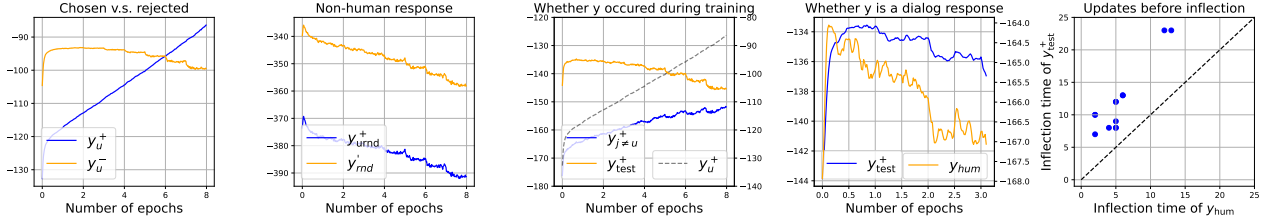


Figure 3: Comparison of the learning dynamics of responses in different groups in the proposed probing dataset (the curve demonstrates the average of the likelihood of all corresponding responses). The last panel compares the inflection time of curves on $\pi_{\theta^t}(\mathbf{y}_{\text{hum}})$ and $\pi_{\theta^t}(\mathbf{y}_{\text{test}}^+)$ under 10 different settings. Results for UltraFeedback are in Figure 9; results under more settings are in Appendix B.2.

partially from) $\mathcal{Y}_{\text{non-IF}}$ in non-negligible, which might cause hallucinations (i.e., using the fact in problem j 's response to answer question i).

We first compare the curves of $\pi_{\theta^t}(\mathbf{y}_{j \neq u}^+)$ and $\pi_{\theta^t}(\mathbf{y}_{\text{test}}^+)$, as illustrated in the third panel in Figure 3. The main difference between them is that the response $\mathbf{y}_{j \neq u}^+$ does occur during training, while $\mathbf{y}_{\text{test}}^+$ does not. Then based on Equation (6), the update of $[\mathbf{x}_{j \neq u}; \mathbf{y}_{j \neq u}^+]$ will influence model's prediction on the combined $[\mathbf{x}_u; \mathbf{y}_{j \neq u}^+]$. That is why $\pi_{\theta^t}(\mathbf{y}_{j \neq u}^+)$ keeps increasing with a slower speed than $\pi_{\theta^t}(\mathbf{y}_u^+)$ all the time, even when the model becomes overfitting. On the contrary, the curve of $\pi_{\theta^t}(\mathbf{y}_{\text{test}}^+)$ first increases for several updates and then begins to decrease as the model keeps training, showing a similar trend as $\pi_{\theta^t}(\mathbf{y}_u^-)$. As these responses never occur during training, there is no consistent upward pressure to counter the downward pressure generated from increasing other responses. That is why these curves go down in the overfitting stage.

We now compare the nuanced difference between $\pi_{\theta^t}(\mathbf{y}_{\text{test}}^+)$ and $\pi_{\theta^t}(\mathbf{y}_{\text{hum}})$, neither of which appears during training. They both have a reverse bell-shaped curve, but the inflection point of $\pi_{\theta^t}(\mathbf{y}_{\text{hum}})$ is consistently earlier than that of $\pi_{\theta^t}(\mathbf{y}_{\text{test}}^+)$, as illustrated in the last two panels of Figure 3. This phenomenon can also support our analysis: since the strength of their downward pressure is at the same level, reaching the plateau earlier means the upward pressure diminishes faster. Recall that $\mathbf{y}_{\text{test}}^+$ also comes from the dataset, while \mathbf{y}_{hum} is randomly generated by GPT4. By examining these responses in \mathbf{y}_{hum} , we find that $\mathbf{y}_{\text{test}}^+$ is more likely to be a "multi-turn dialog response," while the \mathbf{y}_{hum} is usually a descriptive sentence on a random topic (as demonstrated in Figure 8). In other words, \mathcal{K}^t for the former response is likely to be larger, explaining the aforementioned observations.

In summary, the learning dynamics of SFT on different responses could be roughly illustrated by the trend depicted in Figure 2: the model's prediction on most $\mathbf{y} \in \mathcal{Y}_{\text{IF}}$ will be pulled up slightly at the beginning of SFT. Then after several updates, all the responses that never appear in the training set will gradually be pushed down. Note that $\mathbf{y}_{j \neq u}^+ \in \mathcal{Y}_{\text{non-IF}}$ also consistently increases during SFT, which might be a source of hallucination. A more fine-grind analysis considering different rephrases of these responses and the results on different models can be found in Appendix B.

5 Learning Dynamics of LLM Preference Finetuning

Instruction tuning as in the SFT stage above improves the model's instruction-following ability. In order to better align LLM's output with human preferences, typically instruction tuning is followed by preference tuning (Ouyang et al. 2022). The first widespread preference tuning method comes from RLHF (reinforcement learning with human feedback (Christiano et al. 2017)), which requires substantial expert annotation of LLM responses. RLAIF (H. Lee et al. 2023) offload this hard work by collecting preference signals from AI, but a large reward model is still required. To avoid this and mitigate the high-variance nature of the RL-based training, Rafailov et al. (2023) propose DPO (direct preference optimization, an RL-free method), and show it has the same optimization target as RLHF under the Bradley-Terry reward model (R. A. Bradley and Terry 1952). RL-free preference-tuning methods like DPO and variants such as IPO (Azar et al. 2024), SLiC (Zhao et al. 2023), KTO (Ethayarajh et al. 2024), and so on have gained popularity due to their good performance and robustness during training. Significant effort (e.g. Ji et al. 2024; Pal et al. 2024; Rafailov et al. 2024; Tajwar et al. 2024) has gone to theoretical explanations of the equivalence and differences between them and the RL-based methods. This

paper provides a different perspective, understanding these RL-free methods from the gradient space and the learning dynamics. The behavior of all of these methods – even on-policy versions and the instruction tuning method SPIN (Z. Chen et al. 2024) – can be well explained by a similar pipeline as we used for analyzing SFT. We hope the proposed framework can shed more light on how these RL-free methods work and further inspire more efficient algorithms.

5.1 Learning Dynamics of RL-free Preference Tuning: DPO as an Example

We start from the off-policy DPO with the following loss function:

$$\mathcal{L}_{\text{DPO}}(\theta) = - \sum_{(\mathbf{x}_u, \mathbf{y}_u^+, \mathbf{y}_u^-)} \log \sigma \left(\beta \log \frac{\pi_{\theta^t}(\mathbf{y}_u^+ | \mathbf{x}_u)}{\pi_{\text{ref}}(\mathbf{y}_u^+ | \mathbf{x}_u)} - \beta \log \frac{\pi_{\theta^t}(\mathbf{y}_u^- | \mathbf{x}_u)}{\pi_{\text{ref}}(\mathbf{y}_u^- | \mathbf{x}_u)} \right), \quad (8)$$

where \mathbf{y}_u^+ and \mathbf{y}_u^- are pre-generated responses (both in \mathcal{Y}_{IF}), and π_{ref} is the reference model, typically the result of SFT. In the loss function, the π_{θ^t} terms are also calculated using the “teacher forcing” mechanism, which is identical to the SFT case. Hence we decompose the learning dynamics for DPO similarly to Equation (6):

$$[\Delta \log \pi^t(\mathbf{y} | \boldsymbol{\chi}_o)]_m = - \sum_{l=1}^L \eta [\mathcal{A}^t(\boldsymbol{\chi}_o)]_m [\mathcal{K}^t(\boldsymbol{\chi}_o, \tilde{\boldsymbol{\chi}}_u)]_l [\mathcal{G}_{\text{DPO}}^t(\mathbf{x}_u, \mathbf{y}_u^+, \mathbf{y}_u^-)]_l + O(\eta^2) \quad (9)$$

$$\mathcal{G}_{\text{DPO}}^t \approx \beta(1-a)(\mathbf{y}_u^- - \mathbf{y}_u^+); \quad a = \sigma \left(\beta \log \frac{\pi_{\theta^t}(\mathbf{y}_u^+ | \mathbf{x}_u)}{\pi_{\theta^t}(\mathbf{y}_u^- | \mathbf{x}_u)} - \beta \log \frac{\pi_{\text{ref}}(\mathbf{y}_u^+ | \mathbf{x}_u)}{\pi_{\text{ref}}(\mathbf{y}_u^- | \mathbf{x}_u)} \right) \in \mathbb{R} \quad (10)$$

where $\mathcal{K}^t(\boldsymbol{\chi}_o, \tilde{\boldsymbol{\chi}}_u)$ is the *equivalent eNTK* between the updating sequence $[\mathbf{x}_u; \mathbf{y}_u^+, \mathbf{y}_u^-]$ and the observing sequence $[\boldsymbol{\chi}_o; \mathbf{y}_o]$. The derivation, which is similar to before, and the \mathcal{G}^t functions for other RL-free methods are given in Appendix A.2.2.

5.2 Comparison of SFT, DPO, and other Variants

By comparing the learning dynamics of SFT and DPO, we find they have identical \mathcal{A}^t and similar \mathcal{K}^t . The main difference lies in \mathcal{G}^t , which determines the direction and strength of the evolution of π_{θ^t} . Recall the learning dynamics of SFT in the first panel of Figure 4, the pressures controlled by \mathcal{G}^t contain a big positive vector on \mathbf{y}_u^+ and many small negative vectors on other \mathbf{y} , where the positive vector will gradually diminish with the increase of $\pi_{\theta^t}(\mathbf{y}_u^+ | \mathbf{x}_u)$ during training.

The DPO loss, on the other hand, consistently generates a pair of vectors (a positive \mathbf{y}_u^+ and a negative \mathbf{y}_u^-) regardless of the predictions of any policy network². However, as illustrated in Equation (10), the norm of $\mathcal{G}_{\text{DPO}}^t$ is controlled by a scalar $\beta(1-a)$, which is influenced by both the current policy π_{θ^t} and the reference policy π_{ref} . We first analyze the role of a , which is controlled by the margin (i.e., the value inside the parentheses of $\sigma(\cdot)$) that represents how well the current policy separates \mathbf{y}_u^+ and \mathbf{y}_u^- compared with the reference policy. Due to the monotonicity of $\sigma(\cdot)$, a larger margin leads to larger a , which in turn restrains the strength of $\mathcal{G}_{\text{DPO}}^t$. In other words, $\mathcal{G}_{\text{DPO}}^t$ automatically provides less energy on the examples that are already well separated. We then check the role of β , which controls the regularizing effect on the KL distance between π_{θ^t} and π_{ref} in the original RL loss (Rafailov et al. 2023). When the margin is smaller than zero, larger β leads to a smaller a and hence provides stronger $\mathcal{G}_{\text{DPO}}^t$ for the model to “catch up” the separating ability of the reference model faster. But when the model is good enough (the margin is positive), increasing β will increase a and hence create a negative influence on $\beta(1-a)$, which makes the model update less. This behavior aligns well with the claims of Rafailov et al. (2023): the stronger regularizing effect tends to “drag π_{θ} back towards π_{ref} ” when it deviates from π_{ref} too much in terms of the separating capability.

Note that the analyses above don’t make any assumptions on where \mathbf{y}_u^+ and \mathbf{y}_u^- come from. Hence our framework can also be extended to on-policy RL-free algorithms, which often perform better than their off-policy counterparts (Guo, B. Zhang, et al. 2024; Tajwar et al. 2024). By definition, the main difference between off-policy and on-policy algorithms is how the supervisory responses are generated. Off-policy methods typically use a fixed pre-collected dataset, where \mathbf{y}_u^+ and \mathbf{y}_u^- are usually generated by another LLM or humans. In other words, it is likely that both the chosen and rejected responses come from the “less likely” region of the model’s

²Strictly, there should be some small adapting vectors (both positive and negative) on other dimensions in DPO, because the precise $\mathcal{G}_{\text{DPO}}^t$ should contain $(\pi_{\theta^t}(\mathbf{y}_u^+) - \mathbf{y}_u^+) - (\pi_{\theta^t}(\mathbf{y}_u^-) - \mathbf{y}_u^-)$. However, we canceled the π terms to make the expression more concise, using the fact that the model usually pays more attention to response pairs that are not well separated yet.

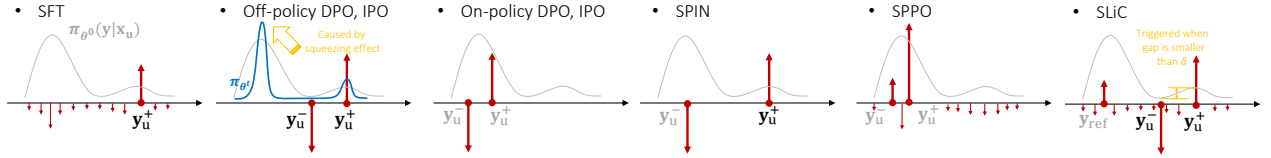


Figure 4: Illustration of the updating vector provided by the residual term \mathcal{G}^t of different algorithms. The gray \mathbf{y} are responses *sampled* from π in an on-policy way. In the second panel, we demonstrate the “squeezing effect” caused by imposing a big negative gradient on a “valley” region of a distribution. For more details about this counter-intuitive effect, please refer to Section 5.3 and Appendix C. For other panels, we demonstrate SPIN (Z. Chen et al. 2024), SPPO (Y. Wu et al. 2024), and SLiC (Zhao et al. 2023).

prediction, as illustrated in the second panel in Figure 4. On-policy responses, on the other hand, are more likely to have higher predicted probabilities under this model, as they were sampled from it. We will show soon that *imposing large negative pressure on an unlikely prediction will lead to unexpected behaviors*. This leads to a unique explanation of why on-policy sampling is so important for algorithms with large negative gradients.

5.3 The Squeezing Effect of the Negative Gradient

The existence of negative gradients (the \mathbf{y}_u^- term in Equation (10)) is the key to understanding the difference of learning dynamics between SFT and DPO. We find this negative gradient will impose a non-trivial “squeezing effect” on any models outputting the probabilistic distribution using Softmax output heads, even in a simple multi-class logistic regression task. Specifically, consider the $L = 1$ case and assume our algorithm imposes a negative gradient on label \bar{y} , the model’s predictive distribution $\pi_{\theta^{t+1}}$ will change as follows:

- The negative gradient will reliably decrease the confidence of \bar{y} , i.e., $\pi_{\theta^{t+1}}(y = \bar{y})$ is guaranteed to decrease.
- The decreased probability mass is “squeezed” into the most confident dimension before the update, i.e., $\pi_{\theta^{t+1}}(y = y^*)$, where $y^* = \operatorname{argmax}_{i \in [V] \setminus \{\bar{y}\}} \pi_{\theta^t}(y = i)$ is guaranteed to increase.
- The rich get richer and the poor get poorer: generally, dimensions with high π_{θ^t} tend to increase, and those with low π_{θ^t} tend to decrease.
- Peakier π_{θ^t} suffer a more serious squeezing effect. If the probability mass concentrates on few dimensions in π_{θ^t} , which is common for a pretrained model, all $\pi_{\theta^{t+1}}(y \neq y^*)$ decrease (only y^* is considered “rich”).
- Smaller $\pi_{\theta^t}(\bar{y})$ make the squeezing effect stronger. If \bar{y} is unlikely under π_{θ^t} , the probability mass of all other $\pi_{\theta^{t+1}}(y \neq y^*)$ will be more seriously decreased, and the $\pi_{\theta^{t+1}}(y = y^*)$ increases more. That is what we observed in the off-policy DPO scenario.

Appendix C proves these observations analytically for linear models, by directly computing $\pi_{\theta^{t+1}}/\pi_{\theta^t}$ in different situations. Intuitively, recall that the cross-entropy loss for a one-hot label \mathbf{e}_i is just $-\log \pi_i = -z_i + \log \sum_j \exp(z_j)$, which has gradient $-\mathbf{e}_i + \pi$. Suppose there is one $k \neq i$ such that π_k is rather large, say 0.8. Then gradient ascent will decrease z_i , but increase z_k almost as much. Since π_k is dominant, increasing its logit results in a large absolute increase to π_k , which necessarily reduces all other probabilities to account for it.

In the next subsection, we will verify these claims by experiments on real LLM finetuning problems. With the help of these analyses, we figure out why the model’s confidence in all responses decreases during off-policy DPO training and successfully find where the decreased probability mass has gone.

5.4 Experimental Analysis of DPO’s Learning Dynamics

To verify our framework also explains the learning dynamics of preference tuning well, we conduct similar experiments for DPO as we do for SFT. Recall the residual term $\mathcal{G}_{\text{DPO}}^t$ introduces a positive arrow on \mathbf{y}_u^+ , which means the learning tries to “pull up” the model’s prediction on \mathbf{y}_u^+ . To verify this, we create two types of rephrases of \mathbf{y}_u^+ using GPT4 and call them $\mathbf{y}_{\text{gpts}}^+$ and $\mathbf{y}_{\text{gptf}}^+$ (the first tend to keep the semantics while the latter tends to keep the format of \mathbf{y}_u^+ ; details in Figure 6). See the three curves in the first panel in Figure 5,

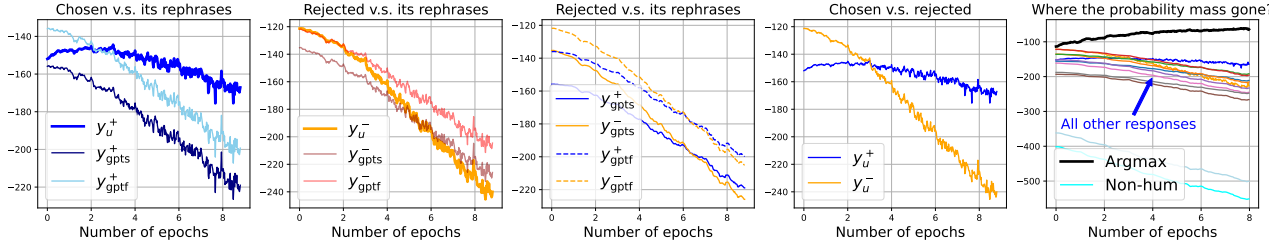


Figure 5: Learning dynamics of off-policy DPO. For experiments on different settings and the results of conducting DPO after SFT, please refer to Appendix B.3.

where the two rephrases decrease at a similar speed, faster than the decay of \mathbf{y}_u^+ . That is because the upward pressure is directly imposed on \mathbf{y}_u^+ rather than these rephrases. Similarly, in the second panel, we observe that \mathbf{y}_u^- decays faster than its rephrases, because $\mathcal{G}_{\text{DPO}}^t$ directly imposes a negative pressure on \mathbf{y}_u^- . Then in the third panel, we find the rephrases of \mathbf{y}_u^+ consistently decay slower than those of \mathbf{y}_u^- , although none of them ever occur during training. That is because these responses are close to \mathbf{y}_u^+ or \mathbf{y}_u^- in \mathcal{Y} , which means the norm of their \mathcal{K}^t is relatively large. Hence the pressures imposed on \mathbf{y}_u^+ and \mathbf{y}_u^- also introduce a non-negligible influence on them. Last, by observing the fourth panel, we find the margin, i.e., $\pi_{\theta^t}(\mathbf{y}_u^+) - \pi_{\theta^t}(\mathbf{y}_u^-)$, keeps increasing, which means the model is gaining the ability to separate \mathbf{y}_u^+ and \mathbf{y}_u^- as the training goes on.

However, although the margin keeps increasing as training continues, the model becomes less confident on *both* \mathbf{y}_u^+ and \mathbf{y}_u^- , as well as on all other responses in the probing dataset. This is different from SFT and quite counter-intuitive: *if everything we observe is becoming less confident, where has the probability mass gone?* The observation has been made by several recent papers (Pal et al. 2024; Rafailov et al. 2024; Tajwar et al. 2024)³ and can be well explained by analyzing a “squeezing effect” of a large negative gradient on \mathbf{y}_u^- . In short, when the negative gradient is imposed on an unlikely prediction under the model (which is very likely in off-policy DPO), the probability mass on almost all responses will be significantly pulled down, and is “squeezed” to the token with the highest confidence. This effect is a basic property of the cross-entropy loss and the Softmax function, which applies to any LLM with softmax heads. Section 5.3 and Appendix C has a full discussion.

To verify this hypothesis, we report the log-likelihood of \mathbf{y} chosen by greedy decoding: each token is chosen by maximizing the conditional probability given $[\mathbf{x}_u; \mathbf{y}_{1:l-1}^+]$, where $\mathbf{y}_{1:l-1}^+$ is a sub-sequence of \mathbf{y}_u^+ . As illustrated by the last panel of Figure 5, the confidence of this “teacher forcing” greedy \mathbf{y} increases very fast (from -113 to -63), which is even faster than the increase of $\pi_{\theta^t}(\mathbf{y}_u^+)$ during SFT (from -130 to -90). However, the tokens with the highest confidence do not necessarily form a preferred response: it will reinforce the prior bias contained in θ^0 . This could be a reasonable explanation of the “degeneration” reported in recent work (e.g. Holtzman et al. 2020): as π_{θ^t} becomes more peaky at its most confident predictions, it is easier to sample sequences with repeated phrases. Note that such behavior could also be understood as a special type of self-bias amplifying (Ren et al. 2024), which would bring more serious consequences if it is combined with a multiple-generation self-improving algorithm, e.g., self-reward (Yuan et al. 2024), iterative DPO (Xiong et al. 2024), etc.

6 Inspirations from Learning Dynamics

Explaining the success of various related algorithms. The proposed learning dynamics explain many interesting observations during SFT and DPO; this perspective also helps explain the success of many practical algorithms. For example, the literature mostly credits on-policy RL-free methods with better aligning the current policy’s distribution to the reward model (Tajwar et al. 2024), but we can extend this explanation from the learning dynamics perspective. As illustrated in the third panel in Figures 4 and 18, we see \mathbf{y}_u^- is sampled from the current π_{θ^t} , which is less likely to be in a valley. Hence the squeezing effect introduced via the big negative gradient is reduced. The benefits of SPIN (Z. Chen et al. 2024), which is inspired by treating the LLM itself as a GAN-style system (Goodfellow et al. 2014), can also be explained similarly: as the negative response \mathbf{y}_u^- always comes from the model’s policy in the previous generation, its π_{θ^t} is less likely to be very

³Particularly in Figure 3 of (Rafailov et al. 2024), where $\pi_{\theta^t}(\mathbf{y}_u^+)$ and $\pi_{\theta^t}(\mathbf{y}_u^-)$ decays even faster if we SFT the model before DPO. This phenomenon can be well explained by the “squeezing effect” discussed in Appendix C.

small. The SPPO method (Y. Wu et al. 2024) even avoids imposing the negative gradient on the model by creating two updating vectors with different lengths (i.e., it improves the confidence on both \mathbf{y}_u^+ and \mathbf{y}_u^- , but at different strength). The success of SLiC (Zhao et al. 2023), whose loss is more complicated than DPO, can also be explained in our framework because its residual term $\mathcal{G}_{\text{SLiC}}^t$ has a similar form as $\mathcal{G}_{\text{DPO}}^t$, as in Equation (24). The threshold δ not only guarantees the π_{θ^t} can learn to separate all \mathbf{y}_u^+ and \mathbf{y}_u^- pairs in the training set with a sufficiently large margin, it also stops imposing a big negative gradient on \mathbf{y}_u^- when the model already has a good separation, where $\pi_{\theta^t}(\mathbf{y}_u^-)$ is likely to be very small. In short, although there are many more RL-free methods and we cannot elaborate on them all in this paper, we believe the analysis proposed can shed more light on their behaviors.

A simple yet effective method. We also propose a simple practical method to verify our theory further. Since the “squeezing effect” of the big negative gradient on unlikely predictions can damage the model’s performance, we can first train the model on *both* $[\mathbf{x}_u; \mathbf{y}_u^+]$ and $[\mathbf{x}_u; \mathbf{y}_u^-]$ during the SFT stage (making the negative response *more* likely), and then run the usual DPO. Following the analysis of Section 4, we can expect the \mathcal{Y}_{IF} region, including \mathbf{y}_u^- , to be pulled up more than with the baseline SFT. To compare, we consider a baseline of standard off-policy DPO (i.e., SFT only on $[\mathbf{x}_u; \mathbf{y}_u^+]$, then DPO). Compared with the baseline, we find the proposed method has more stable learning dynamics that match our analysis well, generates fewer “degenerate” responses, and generates responses that are preferred to those of the baseline almost 70% of the time. Appendix D has more details. In the future, this simple method inspired by our analysis could be further improved by introducing more responses, e.g., rephrases of \mathbf{y}_u^+ , etc., during both stages, and also by combining with many existing methods we mentioned before.

7 Conclusion

Learning dynamics, which depicts how the model’s prediction changes when it learns new examples, provide a powerful tool to analyze the behavior of models trained with gradient descent. To better use this tool in the context of LLM finetuning, we first derive the step-wise decomposition of LLM finetuning for various common algorithms. Then, we propose a unified framework for understanding LLM predictions’ behaviors across different finetuning methods. The proposed analysis successfully explains various phenomena during LLM’s instruction tuning and preference tuning, some of them are quite counter-intuitive. We also shed light on how specific hallucinations are introduced in the SFT stage, as previously observed (Gekhman et al. 2024), and where the improvements of some new RL-free algorithms come from compared with the default off-policy DPO. Finally, inspired by this analysis, we propose a simple (but counter-intuitive) method that is effective in improving the alignment of models.

Acknowledgements

This research was enabled in part by support provided by the Canada CIFAR AI Chairs program, WestGrid, and Compute Canada. We also acknowledge the inspiring discussion with Hamed Shirzad and Shangmin Guo.

References

- Sanjeev Arora, Simon S. Du, Wei Hu, Zhiyuan Li, Ruslan Salakhutdinov, and Ruosong Wang (2019). “On Exact Computation with an Infinitely Wide Neural Net.” *NeurIPS*. arXiv: 1904.11955.
- Mohammad Gheshlaghi Azar, Zhaohan Daniel Guo, Bilal Piot, Remi Munos, Mark Rowland, Michal Valko, and Daniele Calandriello (2024). “A general theoretical paradigm to understand learning from human preferences.” *International Conference on Artificial Intelligence and Statistics*. PMLR, pages 4447–4455.
- Jinze Bai, Shuai Bai, Yunfei Chu, Zeyu Cui, Kai Dang, Xiaodong Deng, Yang Fan, Wenbin Ge, Yu Han, Fei Huang, Binyuan Hui, Luo Ji, Mei Li, Junyang Lin, Runji Lin, Dayiheng Liu, Gao Liu, Chengqiang Lu, Keming Lu, Jianxin Ma, Rui Men, Xingzhang Ren, Xuancheng Ren, Chuanqi Tan, Sinan Tan, Jianhong Tu, Peng Wang, Shijie Wang, Wei Wang, Shengguang Wu, Benfeng Xu, Jin Xu, An Yang, Hao Yang, Jian Yang, Shusheng Yang, Yang Yao, Bowen Yu, Hongyi Yuan, Zheng Yuan, Jianwei Zhang, Xingxuan Zhang, Yichang Zhang, Zhenru Zhang, Chang Zhou, Jingren Zhou, Xiaohuan Zhou, and Tianhang Zhu (2023). “Qwen Technical Report.” arXiv: 2309.16609.

- Yuntao Bai, Andy Jones, Kamal Ndousse, Amanda Askell, Anna Chen, Nova DasSarma, Dawn Drain, Stanislav Fort, Deep Ganguli, Tom Henighan, et al. (2022). “Training a helpful and harmless assistant with reinforcement learning from human feedback.” arXiv: [2204.05862](#).
- Stella Biderman, Hailey Schoelkopf, Quentin Gregory Anthony, Herbie Bradley, Kyle O’Brien, Eric Hallahan, Mohammad Aflah Khan, Shivanshu Purohit, USVSN Sai Prashanth, Edward Raff, et al. (2023). “Pythia: A suite for analyzing large language models across training and scaling.” *ICML*. PMLR, pages 2397–2430.
- Ralph Allan Bradley and Milton E Terry (1952). “Rank analysis of incomplete block designs: I. The method of paired comparisons.” *Biometrika* 39.3/4, pages 324–345.
- Zixiang Chen, Yihe Deng, Huizhuo Yuan, Kaixuan Ji, and Quanquan Gu (2024). “Self-play fine-tuning converts weak language models to strong language models.” arXiv: [2401.01335](#).
- Paul F Christiano, Jan Leike, Tom Brown, Miljan Martic, Shane Legg, and Dario Amodei (2017). “Deep reinforcement learning from human preferences.” *NeurIPS*.
- Ganqu Cui, Lifan Yuan, Ning Ding, Guanming Yao, Wei Zhu, Yuan Ni, Guotong Xie, Zhiyuan Liu, and Maosong Sun (2023). “UltraFeedback: Boosting Language Models with High-quality Feedback.” arXiv: [2310.01377 \[cs.CL\]](#).
- Kawin Ethayarajh, Winnie Xu, Niklas Muennighoff, Dan Jurafsky, and Douwe Kiela (2024). “Kto: Model alignment as prospect theoretic optimization.” arXiv: [2402.01306](#).
- Dan Feldman (2020). “Introduction to core-sets: an updated survey.” arXiv: [2011.09384](#).
- Stanislav Fort, Gintare Karolina Dziugaite, Mansheej Paul, Sepideh Kharaghani, Daniel M Roy, and Surya Ganguli (2020). “Deep learning versus kernel learning: an empirical study of loss landscape geometry and the time evolution of the neural tangent kernel.”
- Zorik Gekhman, Gal Yona, Roei Aharoni, Matan Eyal, Amir Feder, Roi Reichart, and Jonathan Herzig (2024). “Does Fine-Tuning LLMs on New Knowledge Encourage Hallucinations?” arXiv: [2405.05904](#).
- Ian Goodfellow, Jean Pouget-Abadie, Mehdi Mirza, Bing Xu, David Warde-Farley, Sherjil Ozair, Aaron Courville, and Yoshua Bengio (2014). “Generative adversarial nets.” *NeurIPS*.
- Shangmin Guo, Yi Ren, Stefano V Albrecht, and Kenny Smith (2024). “Sample Relationship from Learning Dynamics Matters for Generalisation.” *ICLR*.
- Shangmin Guo, Biao Zhang, Tianlin Liu, Tianqi Liu, Misha Khalman, Felipe Llinares, Alexandre Rame, Thomas Mesnard, Yao Zhao, Bilal Piot, et al. (2024). “Direct language model alignment from online AI feedback.” arXiv: [2402.04792](#).
- Geoffrey Hinton, Oriol Vinyals, and Jeff Dean (2015). “Distilling the knowledge in a neural network.” arXiv: [1503.02531](#).
- Ari Holtzman, Jan Buys, Li Du, Maxwell Forbes, and Yejin Choi (2020). “The Curious Case of Neural Text Degeneration.” *ICLR*.
- Lei Huang, Weijiang Yu, Weitao Ma, Weihong Zhong, Zhangyin Feng, Haotian Wang, Qianglong Chen, Weihua Peng, Xiaocheng Feng, Bing Qin, et al. (2023). “A survey on hallucination in large language models: Principles, taxonomy, challenges, and open questions.” arXiv: [2311.05232](#).
- Arthur Jacot, Franck Gabriel, and Clément Hongler (2018). “Neural tangent kernel: Convergence and generalization in neural networks.” *NeurIPS*.
- Haozhe Ji, Cheng Lu, Yilin Niu, Pei Ke, Hongning Wang, Jun Zhu, Jie Tang, and Minlie Huang (2024). “Towards Efficient and Exact Optimization of Language Model Alignment.” arXiv: [2402.00856](#).
- Ananya Kumar, Aditi Raghunathan, Robbie Matthew Jones, Tengyu Ma, and Percy Liang (2022). “Fine-Tuning can Distort Pretrained Features and Underperform Out-of-Distribution.” *ICLR*.
- Yann LeCun, Léon Bottou, Yoshua Bengio, and Patrick Haffner (1998). “Gradient-based learning applied to document recognition.” *Proceedings of the IEEE* 86.11, pages 2278–2324.
- Harrison Lee, Samrat Phatale, Hassan Mansoor, Kellie Lu, Thomas Mesnard, Colton Bishop, Victor Carbune, and Abhinav Rastogi (2023). “Rlaif: Scaling reinforcement learning from human feedback with ai feedback.” arXiv: [2309.00267](#).
- Jaehoon Lee, Lechao Xiao, Samuel Schoenholz, Yasaman Bahri, Roman Novak, Jascha Sohl-Dickstein, and Jeffrey Pennington (2019). “Wide Neural Networks of Any Depth Evolve as Linear Models Under Gradient Descent.” *NeurIPS*.
- Sheng Liu, Jonathan Niles-Weed, Narges Razavian, and Carlos Fernandez-Granda (2020). “Early-learning regularization prevents memorization of noisy labels.” *NeurIPS*.
- Mohamad Amin Mohamadi, Wonho Bae, and Danica J. Sutherland (2022). “Making Look-Ahead Active Learning Strategies Feasible with Neural Tangent Kernels.” *NeurIPS*. arXiv: [2206.12569](#).

- Long Ouyang, Jeffrey Wu, Xu Jiang, Diogo Almeida, Carroll Wainwright, Pamela Mishkin, Chong Zhang, Sandhini Agarwal, Katarina Slama, Alex Ray, et al. (2022). “Training language models to follow instructions with human feedback.” *NeurIPS*, pages 27730–27744.
- Arka Pal, Deep Karkhanis, Samuel Dooley, Manley Roberts, Siddhartha Naidu, and Colin White (2024). “Smaug: Fixing Failure Modes of Preference Optimisation with DPO-Positive.” arXiv: [2402.13228](#).
- Garima Pruthi, Frederick Liu, Satyen Kale, and Mukund Sundararajan (2020). “Estimating training data influence by tracing gradient descent.” *NeurIPS*.
- Rafael Rafailov, Joey Hejna, Ryan Park, and Chelsea Finn (2024). “From r to Q^* : Your Language Model is Secretly a Q-Function.” arXiv: [2404.12358](#).
- Rafael Rafailov, Archit Sharma, Eric Mitchell, Christopher D Manning, Stefano Ermon, and Chelsea Finn (2023). “Direct preference optimization: Your language model is secretly a reward model.” *NeurIPS*.
- Yi Ren, Shangmin Guo, Wonho Bae, and Danica J. Sutherland (2023). “How to prepare your task head for finetuning.” *ICLR*.
- Yi Ren, Shangmin Guo, Matthieu Labeau, Shay B. Cohen, and Simon Kirby (2020). “Compositional languages emerge in a neural iterated learning model.” *ICLR*.
- Yi Ren, Shangmin Guo, Linlu Qiu, Bailin Wang, and Danica J Sutherland (2024). “Language Model Evolution: An Iterated Learning Perspective.” arXiv: [2404.04286](#).
- Yi Ren, Shangmin Guo, and Danica J. Sutherland (2022). “Better Supervisory Signals by Observing Learning Paths.” *ICLR*.
- Yi Ren, Samuel Lavoie, Michael Galkin, Danica J Sutherland, and Aaron C Courville (2023). “Improving compositional generalization using iterated learning and simplicial embeddings.” *NeurIPS*.
- Burr Settles (2009). “Active learning literature survey.”
- Fahim Tajwar, Anikait Singh, Archit Sharma, Rafael Rafailov, Jeff Schneider, Tengyang Xie, Stefano Ermon, Chelsea Finn, and Aviral Kumar (2024). “Preference Fine-Tuning of LLMs Should Leverage Suboptimal, On-Policy Data.” arXiv: [2404.14367 \[cs.LG\]](#).
- Ashish Vaswani, Noam Shazeer, Niki Parmar, Jakob Uszkoreit, Llion Jones, Aidan N. Gomez, Lukasz Kaiser, and Illia Polosukhin (2017). “Attention Is All You Need.” *NeurIPS*. arXiv: [1706.03762](#).
- Tongzhou Wang, Jun-Yan Zhu, Antonio Torralba, and Alexei A Efros (2018). “Dataset distillation.” arXiv: [1811.10959](#).
- Jason Wei, Maarten Bosma, Vincent Zhao, Kelvin Guu, Adams Wei Yu, Brian Lester, Nan Du, Andrew M. Dai, and Quoc V Le (2022). “Finetuned Language Models are Zero-Shot Learners.” *ICLR*.
- Yue Wu, Zhiqing Sun, Huizhuo Yuan, Kaixuan Ji, Yiming Yang, and Quanquan Gu (2024). “Self-play preference optimization for language model alignment.” arXiv: [2405.00675](#).
- Mengzhou Xia, Sadhika Malladi, Suchin Gururangan, Sanjeev Arora, and Danqi Chen (2024). “Less: Selecting influential data for targeted instruction tuning.” arXiv: [2402.04333](#).
- Wei Xiong, Hanze Dong, Chenlu Ye, Ziqi Wang, Han Zhong, Heng Ji, Nan Jiang, and Tong Zhang (2024). “Iterative Preference Learning from Human Feedback: Bridging Theory and Practice for RLHF under KL-constraint.” *ICML*.
- Zhaorui Yang, Qian Liu, Tianyu Pang, Han Wang, Haozhe Feng, Minfeng Zhu, and Wei Chen (2024). “Self-Distillation Bridges Distribution Gap in Language Model Fine-Tuning.” arXiv: [2402.13669](#).
- Weizhe Yuan, Richard Yuanzhe Pang, Kyunghyun Cho, Sainbayar Sukhbaatar, Jing Xu, and Jason Weston (2024). “Self-rewarding language models.” arXiv: [2401.10020](#).
- Yao Zhao, Rishabh Joshi, Tianqi Liu, Misha Khalman, Mohammad Saleh, and Peter J Liu (2023). “Slic-hf: Sequence likelihood calibration with human feedback.” arXiv: [2305.10425](#).

A Proof of Propositions and Residual Term for Different Losses

A.1 Proof of Proposition 1

Proposition 1 (Similar to Proposition 1 of Ren et al. 2022). *Let $\pi = \text{Softmax}(\mathbf{z})$ and $\mathbf{z} = h_\theta(\mathbf{x})$. The one-step learning dynamics decompose as*

$$\underbrace{\Delta \log \pi^t(\mathbf{y} | \mathbf{x}_o)}_{V \times 1} = -\eta \underbrace{\mathcal{A}^t(\mathbf{x}_o)}_{V \times V} \underbrace{\mathcal{K}^t(\mathbf{x}_o, \mathbf{x}_u)}_{V \times V} \underbrace{\mathcal{G}^t(\mathbf{x}_u, \mathbf{y}_u)}_{V \times 1} + O(\eta^2 \|\nabla_\theta \mathbf{z}(\mathbf{x}_u)\|_{\text{op}}^2), \quad (4)$$

where $\mathcal{A}^t(\mathbf{x}_o) = \nabla_{\mathbf{z}} \log \pi_{\theta^t}(\mathbf{x}_o) = I - \mathbf{1} \pi_{\theta^t}^\top(\mathbf{x}_o)$, $\mathcal{K}^t(\mathbf{x}_o, \mathbf{x}_u) = (\nabla_\theta \mathbf{z}(\mathbf{x}_o)|_{\theta^t})(\nabla_\theta \mathbf{z}(\mathbf{x}_u)|_{\theta^t})^\top$ is the empirical neural tangent kernel of the logit network and $\mathcal{G}^t(\mathbf{x}_u, \mathbf{y}_u) = \nabla_{\mathbf{z}} \mathcal{L}(\mathbf{x}_u, \mathbf{y}_u)|_{\mathbf{z}^t}$, which for cross-entropy loss is $\pi_{\theta^t}(\mathbf{y} | \mathbf{x}_u) - \mathbf{y}_u$.

*Proof.*⁴ Suppose we want to observe the model’s prediction on an “observing example” \mathbf{x}_o . Starting from Equation (3), we first approximate $\log \pi^{t+1}(\mathbf{y} | \mathbf{x}_o)$ using first-order Taylor expansion (we use π^t to represent π_{θ^t} here for notation conciseness):

$$\log \pi^{t+1}(\mathbf{y} | \mathbf{x}_o) = \log \pi^t(\mathbf{y} | \mathbf{x}_o) + \langle \nabla \log \pi^t(\mathbf{y} | \mathbf{x}_o), \theta^{t+1} - \theta^t \rangle + O(\|\theta^{t+1} - \theta^t\|^2).$$

Then, assuming the model updates its parameters using SGD calculated by an “updating example” $(\mathbf{x}_u, \mathbf{y}_u)$, we can rearrange the terms in the above equation to get the following expression:

$$\Delta \log \pi^t(\mathbf{y} | \mathbf{x}_o) = \underbrace{\log \pi^{t+1}(\mathbf{y} | \mathbf{x}_o)}_{V \times 1} - \underbrace{\log \pi^t(\mathbf{y} | \mathbf{x}_o)}_{V \times 1} = \underbrace{\nabla_\theta \log \pi^t(\mathbf{y} | \mathbf{x}_o)|_{\theta^t}}_{V \times d} \underbrace{(\theta^{t+1} - \theta^t)}_{d \times 1} + O(\|\theta^{t+1} - \theta^t\|^2),$$

where d is the number of parameters of the model. To evaluate the leading term, we plug in the definition of SGD and repeatedly use the chain rule:

$$\begin{aligned} \underbrace{\nabla_\theta \log \pi^t(\mathbf{y} | \mathbf{x}_o)|_{\theta^t}}_{V \times d} \underbrace{(\theta^{t+1} - \theta^t)}_{d \times 1} &= \left(\underbrace{\nabla_{\mathbf{z}} \log \pi^t(\mathbf{x}_o)|_{\mathbf{z}^t}}_{V \times V} \underbrace{\nabla_\theta \mathbf{z}^t(\mathbf{x}_o)|_{\theta^t}}_{V \times d} \right) \left(\underbrace{-\eta \nabla_\theta \mathcal{L}(\mathbf{x}_u)|_{\theta^t}}_{1 \times d} \right)^\top \\ &= \underbrace{\nabla_{\mathbf{z}} \log \pi^t(\mathbf{x}_o)|_{\mathbf{z}^t}}_{V \times V} \underbrace{\nabla_\theta \mathbf{z}^t(\mathbf{x}_o)|_{\theta^t}}_{V \times d} \left(\underbrace{-\eta \nabla_{\mathbf{z}} \mathcal{L}(\mathbf{x}_u)|_{\mathbf{z}^t}}_{1 \times V} \underbrace{\nabla_\theta \mathbf{z}^t(\mathbf{x}_u)|_{\theta^t}}_{V \times d} \right)^\top \\ &= -\eta \underbrace{\nabla_{\mathbf{z}} \log \pi^t(\mathbf{x}_o)|_{\mathbf{z}^t}}_{V \times V} \left[\underbrace{\nabla_\theta \mathbf{z}^t(\mathbf{x}_o)|_{\theta^t}}_{V \times d} \underbrace{(\nabla_\theta \mathbf{z}^t(\mathbf{x}_u)|_{\theta^t})^\top}_{d \times V} \right] \underbrace{(\nabla_{\mathbf{z}} \mathcal{L}(\mathbf{x}_u)|_{\mathbf{z}^t})^\top}_{V \times 1} \\ &= -\eta \mathcal{A}^t(\mathbf{x}_o) \mathcal{K}^t(\mathbf{x}_o, \mathbf{x}_u) \mathcal{G}^t(\mathbf{x}_u, \mathbf{y}_u) \end{aligned} \quad (11)$$

For the higher-order term, using as above that

$$\theta^{t+1} - \theta^t = -\eta \nabla_\theta \mathbf{z}^t(\mathbf{x}_u)|_{\theta^t}^\top \mathcal{G}^t(\mathbf{x}_u, \hat{\mathbf{y}})$$

and noting that, since the residual term \mathcal{G}^t is usually bounded (and the practical algorithms will also use gradient clip to avoid too large gradient), we have that

$$O(\|\theta^{t+1} - \theta^t\|^2) = O(\eta^2 \|\nabla_\theta \mathbf{z}^t(\mathbf{x}_u)|_{\theta^t}\|_{\text{op}}^2 \|\mathcal{G}^t(\mathbf{x}_u, \hat{\mathbf{y}})\|^2) = O(\eta^2 \|\nabla_\theta \mathbf{z}(\mathbf{x}_u)\|_{\text{op}}^2). \quad \square$$

In the decomposition, using $\{\pi_1, \dots, \pi_V\}$ to represent the model’s prediction on different dimensions, we can write our \mathcal{A}^t as:

$$\mathcal{A}^t(\mathbf{x}_o) = I - \mathbf{1}(\pi^t)^\top = \begin{bmatrix} 1 - \pi_1 & -\pi_1 & \cdots & -\pi_1 \\ -\pi_2 & 1 - \pi_2 & \cdots & -\pi_2 \\ \cdots & \cdots & \ddots & \cdots \\ -\pi_V & -\pi_V & \cdots & 1 - \pi_V \end{bmatrix}, \quad (12)$$

The second term in this decomposition, $\mathcal{K}^t(\mathbf{x}_o, \mathbf{x}_u)$, is the product of gradients at \mathbf{x}_o and \mathbf{x}_u . Intuitively, if their gradients have similar directions, this matrix is large, and vice versa. This matrix is known as the

⁴Note that this proposition assumes $L = 1$. For $L > 1$ case, we will have multiple task heads which leads to L different Equation (4). The $V \times L$ matrix $\Delta \pi^t$ can then be achieved by stacking them.

empirical neural tangent kernel, and it can change through the course of training as the network’s notion of “similarity” evolves. For appropriately initialized very wide networks trained with very small learning rates, \mathcal{K}^t remains almost constant during the course of training, the kernel it converges to is known as the neural tangent kernel (Arora et al. 2019; Jacot et al. 2018). Note that the assumption that $\mathcal{K}^t(\mathbf{x}_o, \mathbf{x}_u)$ is unchanged (usually used in theoretical analysis) might be too strong in the LLM’s finetuning. However, as stated in many related works (Arora et al. 2019; Ren, Guo, et al. 2023), assuming $\mathcal{K}^t(\mathbf{x}_o, \mathbf{x}_u)$ as a slow-change and almost consistent similarity measurement between \mathbf{x}_o and \mathbf{x}_u from the model’s perspective is reasonable.

A.2 Residual Term for Different LLM Finetuning Algorithms

As stated in Section 4, one of the conundrums of decomposing the learning dynamics of LLM is its auto-regression nature of the output sequence. Different from the multi-label classification problem, where \mathbf{y}_l for different l is independently generated as long as the shared network is fixed, the \mathbf{y}_l for the LLM’s output depends on $\mathbf{y}_{1:l-1}$, which is usually sampled from the model’s prediction iteratively. However, in most of the finetuning cases where the supervisory signal \mathbf{y}_u is given, the model will apply the so-called “teacher forcing” mechanism when calculating the predicting probabilities. In other words, when generating the output of each \mathbf{y}_l , the $\mathbf{y}_{1:l-1}$ is given rather than sampled on-policy. This mechanism makes it possible for us to define $\boldsymbol{\chi} = [\mathbf{x}; \mathbf{y}]$ and hence merge the auto-regressive nature of the sequence prediction into the shared $\mathcal{K}^t(\mathbf{x}_o, \mathbf{x}_u)$. After this step, the decomposition of LLM’s finetuning learning dynamics then becomes similar to a multi-label classification task.

A.2.1 Instruction finetuning using auto-regression loss (SFT)

Here we derive the residual term, i.e., \mathcal{G}^t for different algorithms in LLM’s finetuning. We first rewrite Equation (6) here:

$$\underbrace{[\Delta \log \pi^t(\mathbf{y} | \boldsymbol{\chi}_o)]_m}_{V \times M} = - \sum_{l=1}^L \eta \underbrace{[\mathcal{A}^t(\boldsymbol{\chi}_o)]_m}_{V \times V \times M} \underbrace{[\mathcal{K}^t(\boldsymbol{\chi}_o, \boldsymbol{\chi}_u)]_l}_{V \times V \times L} \underbrace{[\mathcal{G}^t(\boldsymbol{\chi}_u)]_l}_{V \times L} + O(\eta^2), m \in \{1, \dots, M\}, l \in \{1, \dots, L\},$$

where $\mathcal{G}^t(\boldsymbol{\chi}_u) = \nabla_{\mathbf{z}} \mathcal{L}(\boldsymbol{\chi}_u)|_{\mathbf{z}^t}$ is a $V \times L$ matrix. As the auto-regression nature of the SFT loss is already encoded in the causal mask used in h_θ , the columns in $\mathcal{G}^t(\boldsymbol{\chi}_u)$ are independent of each other, which can be separately calculated. Plus, the summation over l can also be achieved by left-multiplying a length- L all-one vector $\mathbf{1}$. Specifically, the SFT loss for each l is:

$$[\mathcal{L}_{\text{SFT}}(\boldsymbol{\chi}_u)]_l = -\log \pi(\mathbf{y}_l = \hat{\mathbf{y}}_l | \boldsymbol{\chi}_u) = -\mathbf{e}_{\hat{\mathbf{y}}_l}^\top \log \pi(\mathbf{y}_l | \boldsymbol{\chi}_u) = -\mathbf{e}_{\mathbf{y}_l^+}^\top \log(\text{Softmax}(\mathbf{z}_l)).$$

The gradient of \mathcal{L} on \mathbf{z} can be then calculated as:

$$\begin{aligned} [\mathcal{G}_{\text{SFT}}^t(\boldsymbol{\chi}_u)]_l &= \underbrace{\nabla_{\mathbf{z}_l} [\mathcal{L}_{\text{SFT}}(\boldsymbol{\chi}_u)]_l}_{1 \times V} = \left(\underbrace{\nabla_{\pi} [\mathcal{L}_{\text{SFT}}(\boldsymbol{\chi}_u)]_l}_{V \times 1} \right)^\top \underbrace{\nabla_{\mathbf{z}_l} \pi}_{V \times V} \\ &= -(\mathbf{e}_{\hat{\mathbf{y}}_l} \oslash \pi)^\top [\mathcal{A}(\boldsymbol{\chi}_u)]_l = \pi(\mathbf{y}_l | \boldsymbol{\chi}_u) - \mathbf{e}_{\mathbf{y}_l^+}, \end{aligned} \quad (13)$$

where \oslash is element-wise division and $[\mathcal{A}(\boldsymbol{\chi}_u)]_l$ has a form like Equation (12). By stacking the terms with different $l \in [L]$, we can get

$$\mathcal{G}_{\text{SFT}}^t(\boldsymbol{\chi}_u) = \nabla_{\mathbf{z}} \mathcal{L}_{\text{SFT}}(\boldsymbol{\chi}_u)|_{\mathbf{z}^t} = \pi_{\theta^t}(\mathbf{y} | \boldsymbol{\chi}_u) - \mathbf{e}_{\mathbf{y}^+}, \quad (14)$$

as stated in Equation (7).

A.2.2 Different preference finetuning algorithms

Direct Preference Optimization (DPO (Rafailov et al. 2023)) is usually considered the first RL-free alignment algorithm for preference finetuning. Different from the standard RLHF (reinforcement learning with human feedback (Christiano et al. 2017)), the training of off-policy DPO is more similar to SFT, where the model keeps learning from a pre-generated preference dataset. We hence start from DPO to analyze the learning dynamics of different preference finetuning algorithms (actually, the on-policy versions of these algorithms could also be explained using the proposed framework).

Following Rafailov et al. 2023, the training loss of DPO is:

$$\mathcal{L}_{\text{DPO}}(\theta) = - \sum_{(\mathbf{x}_u, \mathbf{y}_u^+, \mathbf{y}_u^-)} \log \sigma \left(\beta \log \frac{\pi_{\theta^t}(\mathbf{y}_u^+ | \mathbf{x}_u)}{\pi_{\text{ref}}(\mathbf{y}_u^+ | \mathbf{x}_u)} - \beta \log \frac{\pi_{\theta^t}(\mathbf{y}_u^- | \mathbf{x}_u)}{\pi_{\text{ref}}(\mathbf{y}_u^- | \mathbf{x}_u)} \right). \quad (15)$$

Before calculating the residual term $\mathcal{G}_{\text{DPO}}^t$, we need to re-calculate the learning dynamics decomposition, because the loss term now depends on both $\pi_{\theta^t}(\mathbf{y}_u^+ | \mathbf{x}_u)$ and $\pi_{\theta^t}(\mathbf{y}_u^- | \mathbf{x}_u)$, which involves two different \mathbf{z} terms. Specifically, we define $\pi_{\theta^t}(\mathbf{y}_u^+ | \mathbf{x}_u) = \text{Softmax_column}(\mathbf{z}^+)$ and $\pi_{\theta^t}(\mathbf{y}_u^- | \mathbf{x}_u) = \text{Softmax_column}(\mathbf{z}^-)$, where $\mathbf{z}^+ = h_{\theta}(\boldsymbol{\chi}_u^+)$ and $\mathbf{z}^- = h_{\theta}(\boldsymbol{\chi}_u^-)$ respectively ($\boldsymbol{\chi}_u^+ = [\mathbf{x}_u; \mathbf{y}_u^+]$ and $\boldsymbol{\chi}_u^- = [\mathbf{x}_u; \mathbf{y}_u^-]$). Then, considering the $L = 1$ case, Equation (11) for the DPO loss could be written as:

$$\begin{aligned} \underbrace{\nabla_{\theta} \log \pi^t(\boldsymbol{\chi}_o)}_{V \times d} \underbrace{\Delta \theta^t}_{d \times 1} &= \underbrace{(\nabla_{\mathbf{z}} \log \pi^t(\boldsymbol{\chi}_o) |_{\mathbf{z}^t})}_{V \times V} \underbrace{\nabla_{\theta} \mathbf{z}^t(\boldsymbol{\chi}_o) |_{\theta^t}}_{V \times d} \underbrace{(-\eta \nabla_{\theta} \mathcal{L}(\mathbf{x}_u, \mathbf{y}_u^+, \mathbf{y}_u^-) |_{\theta^t})}_{1 \times d}^{\top} \\ &= \underbrace{\nabla_{\mathbf{z}} \log \pi^t(\boldsymbol{\chi}_o) |_{\mathbf{z}^t}}_{V \times V} \underbrace{\nabla_{\theta} \mathbf{z}^t(\boldsymbol{\chi}_o) |_{\theta^t}}_{V \times d} \underbrace{(-\eta \nabla_{[\mathbf{z}^+; \mathbf{z}^-]} \mathcal{L} |_{\mathbf{z}^t})}_{1 \times 2V} \underbrace{[\nabla_{\theta} \mathbf{z}^+(\boldsymbol{\chi}_u^+); \nabla_{\theta} \mathbf{z}^-(\boldsymbol{\chi}_u^-)] |_{\theta^t}}_{2V \times d}^{\top} \\ &= -\eta \underbrace{\nabla_{\mathbf{z}} \log \pi^t(\boldsymbol{\chi}_o) |_{\mathbf{z}^t}}_{V \times V} \underbrace{[\nabla_{\theta} \mathbf{z}^t(\boldsymbol{\chi}_o) |_{\theta^t}]}_{V \times d} \underbrace{([\nabla_{\theta} \mathbf{z}^+(\boldsymbol{\chi}_u^+); \nabla_{\theta} \mathbf{z}^-(\boldsymbol{\chi}_u^-)] |_{\theta^t})}_{d \times 2V}^{\top} \underbrace{(\nabla_{[\mathbf{z}^+; \mathbf{z}^-]} \mathcal{L} |_{\mathbf{z}^t})}_{2V \times 1}^{\top} \\ &= -\eta \mathcal{A}^t(\boldsymbol{\chi}_o) [\mathcal{K}^t(\boldsymbol{\chi}_o, \boldsymbol{\chi}_u^+); \mathcal{K}^t(\boldsymbol{\chi}_o, \boldsymbol{\chi}_u^-)] (\nabla_{[\mathbf{z}^+; \mathbf{z}^-]} \mathcal{L} |_{\mathbf{z}^t})^{\top} \\ &= -\eta \mathcal{A}^t(\boldsymbol{\chi}_o) \mathcal{K}^t(\boldsymbol{\chi}_o, \tilde{\boldsymbol{\chi}}_u) \mathcal{G}^t(\mathbf{x}_u, \mathbf{y}_u^+, \mathbf{y}_u^-), \end{aligned} \quad (16)$$

where $\mathcal{K}^t(\boldsymbol{\chi}_o, \tilde{\boldsymbol{\chi}}_u)$ is the equivalent eNTK that average the influence of both \mathbf{y}_u^+ and \mathbf{y}_u^- .

We then calculate the residual term \mathcal{G}^t for DPO. For ease of calculation, we decompose the loss into:

$$\begin{aligned} \mathcal{L}_{\text{DPO}}(\mathbf{x}_u, \mathbf{y}_u^+, \mathbf{y}_u^- | \theta) &= -\log(a) \\ a &\triangleq \sigma(b) \\ b &\triangleq \beta (\log \pi_{\theta^t}(\mathbf{y}_u^+) - \log \pi_{\theta^t}(\mathbf{y}_u^-)) - c \\ &= \beta (\mathbf{e}_{\mathbf{y}_u^+} - \mathbf{e}_{\mathbf{y}_u^-})^{\top} \log \pi_{\theta^t}(\mathbf{y} | \mathbf{x}_u) - c \\ &= \beta (\mathcal{L}_{\text{SFT}}([\mathbf{x}_u, \mathbf{y}_u^-]) - \mathcal{L}_{\text{SFT}}([\mathbf{x}_u, \mathbf{y}_u^+])) - c \\ c &\triangleq \beta (\mathbf{e}_{\mathbf{y}_u^+} - \mathbf{e}_{\mathbf{y}_u^-})^{\top} \log \pi_{\text{ref}}(\mathbf{y} | \mathbf{x}_u), \end{aligned} \quad (17)$$

where c is not a function of θ . Using the chain rule, the l -th column of the residual term $\mathcal{G}_{\text{DPO}}^t$ can be calculated as:

$$\begin{aligned} [\mathcal{G}_{\text{DPO}}^t]_l &= \frac{\partial \mathcal{L}_{\text{DPO}}}{\partial a} \frac{\partial a}{\partial b} \nabla_{\pi} b |_{\pi_{\theta^t}} \nabla_{\mathbf{z}_l} \pi^t |_{\mathbf{z}_l^t} \\ &= -\frac{1}{a} a(1-a) \langle \nabla_{\pi} b |_{\pi_{\theta^t}}, [\mathcal{A}^t(\boldsymbol{\chi}_u)]_l \rangle \\ &= -(1-a) \langle \beta (\mathcal{L}_{\text{SFT}}([\mathbf{x}_u, \mathbf{y}_u^-])_l - \mathcal{L}_{\text{SFT}}([\mathbf{x}_u, \mathbf{y}_u^+]_l)), [\mathcal{A}^t(\boldsymbol{\chi}_u)]_l \rangle \\ &= -\beta(1-a) (\langle \mathcal{L}_{\text{SFT}}([\mathbf{x}_u, \mathbf{y}_u^-])_l, [\mathcal{A}^t(\boldsymbol{\chi}_u)]_l \rangle - \langle \mathcal{L}_{\text{SFT}}([\mathbf{x}_u, \mathbf{y}_u^+]_l), [\mathcal{A}^t(\boldsymbol{\chi}_u)]_l \rangle) \\ &= -\beta(1-a) \left((\pi_{\theta^t}(\mathbf{y}_u^-) - \mathbf{e}_{\mathbf{y}_u^-}) - (\pi_{\theta^t}(\mathbf{y}_u^+) - \mathbf{e}_{\mathbf{y}_u^+}) \right)_l \\ &\approx \beta(1-a) (\mathbf{e}_{\mathbf{y}_u^-} - \mathbf{e}_{\mathbf{y}_u^+})_l. \end{aligned} \quad (18)$$

The approximation in the last line takes the fact that at the early stage of alignment, the model might not separate \mathbf{y}_u^+ and \mathbf{y}_u^- well. Hence we can eliminate the influence of $\pi_{\theta^t}(\mathbf{y}_u^-) - \pi_{\theta^t}(\mathbf{y}_u^+)$ to have a more concise expression. By stacking values with different l , we can get the residual term of DPO as

$$\mathcal{G}_{\text{DPO}}^t \approx \beta(1-a) (\mathbf{e}_{\mathbf{y}_u^-} - \mathbf{e}_{\mathbf{y}_u^+}); a = \sigma \left(\beta \log \frac{\pi_{\theta^t}(\mathbf{y}_u^+ | \mathbf{x}_u)}{\pi_{\theta^t}(\mathbf{y}_u^- | \mathbf{x}_u)} - \beta \log \frac{\pi_{\text{ref}}(\mathbf{y}_u^+ | \mathbf{x}_u)}{\pi_{\text{ref}}(\mathbf{y}_u^- | \mathbf{x}_u)} \right) \quad (19)$$

Similarly, we can calculate the residual terms for other off-policy preference optimization methods, like Identity-preference Optimization (IPO (Azar et al. 2024)):

$$\mathcal{L}_{\text{IPO}} = - \sum_{(\mathbf{x}_u, \mathbf{y}_u^+, \mathbf{y}_u^-)} \left(\left(\log \frac{\pi_{\theta^t}(\mathbf{y}_u^+ | \mathbf{x}_u)}{\pi_{\text{ref}}(\mathbf{y}_u^+ | \mathbf{x}_u)} - \log \frac{\pi_{\theta^t}(\mathbf{y}_u^- | \mathbf{x}_u)}{\pi_{\text{ref}}(\mathbf{y}_u^- | \mathbf{x}_u)} - \frac{1}{2\beta} \right) \right)^2. \quad (20)$$

$$\mathcal{G}_{\text{IPO}}^t \approx 2a (\mathbf{e}_{\mathbf{y}_u^-} - \mathbf{e}_{\mathbf{y}_u^+}); a = \log \frac{\pi_{\theta^t}(\mathbf{y}_u^+ | \mathbf{x}_u)}{\pi_{\theta^t}(\mathbf{y}_u^- | \mathbf{x}_u)} - \log \frac{\pi_{\text{ref}}(\mathbf{y}_u^+ | \mathbf{x}_u)}{\pi_{\text{ref}}(\mathbf{y}_u^- | \mathbf{x}_u)} - \frac{1}{2\beta} \quad (21)$$

For the Sequence Likelihood Calibration (SLiC (Zhao et al. 2023)), we have:

$$\mathcal{L}_{\text{SLiC}} = - \sum_{(\mathbf{x}_u, \mathbf{y}_u^+, \mathbf{y}_u^-)} \max \left[0, \delta - \log \frac{\pi_{\theta^t}(\mathbf{y}_u^+ | \mathbf{x}_u)}{\pi_{\theta^t}(\mathbf{y}_u^- | \mathbf{x}_u)} \right] - \beta \cdot \log \pi_{\theta^t}(\mathbf{y}_{\text{ref}} | \mathbf{x}_u) \quad (22)$$

$$= - \sum_{(\mathbf{x}_u, \mathbf{y}_u^+, \mathbf{y}_u^-)} \max [0, \delta + \mathcal{L}_{\text{SFT}}([\mathbf{x}_u, \mathbf{y}_u^+]) - \mathcal{L}_{\text{SFT}}([\mathbf{x}_u, \mathbf{y}_u^-])] + \beta \mathcal{L}_{\text{SFT}}([\mathbf{x}_u, \mathbf{y}_{\text{ref}}]) \quad (23)$$

$$\mathcal{G}_{\text{SLiC}}^t \approx a (\mathbf{e}_{\mathbf{y}_u^-} - \mathbf{e}_{\mathbf{y}_u^+}) + \beta (\pi_{\theta^t}(\mathbf{y} | \mathbf{x}_u) - \mathbf{e}_{\mathbf{y}_{\text{ref}}}); a = \mathbf{1} \left(\delta - \log \frac{\pi_{\theta^t}(\mathbf{y}_u^+)}{\pi_{\theta^t}(\mathbf{y}_u^-)} > 0 \right) \quad (24)$$

In summary, these RL-free algorithms all relate to the SFT loss to some extent. For the DPO and IPO loss, the directions of the updating signals are identical (i.e., $\mathbf{e}_{\mathbf{y}_u^-} - \mathbf{e}_{\mathbf{y}_u^+}$, where the $\pi(\mathbf{y})$ term is canceled during calculation). A scalar controls the strength of this update, which usually correlated with the confidence gap between the model’s current confidence on \mathbf{y}_u^+ and \mathbf{y}_u^- , i.e., $\text{Gap}(\pi_{\theta^t}) \triangleq \log \frac{\pi_{\theta^t}(\mathbf{y}_u^+ | \mathbf{x}_u)}{\pi_{\theta^t}(\mathbf{y}_u^- | \mathbf{x}_u)}$. Generally, larger this value leads to a bigger a , making the norm of \mathcal{G}^t smaller. In other words, we see a “regularizing” effect in this term, where the model should not make $\text{Gap}(\pi_{\theta^t})$ too large. The SLiC loss can be considered as a combination of SFT adaptation and preference adaptation. Similarly, we can also see a hard version of the regularization effect mentioned above. If $\text{Gap}(\pi_{\theta^t}) > \delta$, the indicator function will become zero, and the model stops pushing $\pi(\mathbf{y}_u^+)$ and $\pi(\mathbf{y}_u^-)$ away when it already separates \mathbf{y}_u^+ and \mathbf{y}_u^- well.

Recently, authors of (Y. Wu et al. 2024) propose another interesting self-play alignment algorithm called SPPO, which further improves the alignment performance on top of many on-policy DPO methods. Our framework could also give an interesting explanation of why this method works so well. Specifically, the loss function of SPPO can be written as:

$$\mathcal{L}_{\text{SPPO}} = - \sum_{(\mathbf{x}_u, \mathbf{y}_u^+, \mathbf{y}_u^-)} \left(\log \frac{\pi_{\theta^t}(\mathbf{y}_u^+ | \mathbf{x}_u)}{\pi_{\text{ref}}(\mathbf{y}_u^+ | \mathbf{x}_u)} - \frac{\eta}{2} \right)^2 + \left(\log \frac{\pi_{\theta^t}(\mathbf{y}_u^- | \mathbf{x}_u)}{\pi_{\text{ref}}(\mathbf{y}_u^- | \mathbf{x}_u)} + \frac{\eta}{2} \right)^2. \quad (25)$$

$$\mathcal{G}_{\text{SPPO}}^t = 2 \left(\log \frac{\pi_{\theta^t}(\mathbf{y}_u^+ | \mathbf{x}_u)}{\pi_{\text{ref}}(\mathbf{y}_u^+ | \mathbf{x}_u)} - \frac{\eta}{2} \right) (\pi_{\theta^t} - \mathbf{e}_{\mathbf{y}_u^+}) + 2 \left(\log \frac{\pi_{\theta^t}(\mathbf{y}_u^- | \mathbf{x}_u)}{\pi_{\text{ref}}(\mathbf{y}_u^- | \mathbf{x}_u)} + \frac{\eta}{2} \right) (\pi_{\theta^t} - \mathbf{e}_{\mathbf{y}_u^-}). \quad (26)$$

This loss looks similar to the IPO one, but the main difference between SPPO and other methods (e.g., DPO, KTO, IPO, SPIN, etc.) is that there is no negative sign in front of $\pi_{\theta^t}(\mathbf{y}_u^+ | \mathbf{x}_u)$ or $\pi_{\theta^t}(\mathbf{y}_u^- | \mathbf{x}_u)$. From its residual term $\mathcal{G}_{\text{SPPO}}^t$, it is more convenient to understand this algorithm as imposing two positive vectors on both \mathbf{y}_u^+ and \mathbf{y}_u^- , but the former has a longer norm, as illustrated in Figure 4. By doing so, the big negative gradient no longer exists, and so does the squeezing effect. That is partly why this method is more stable and performs better.

B More Results of Observing the Learning Dynamics

This section provides more experimental results about the learning dynamics to support our claim. We will extend our probing dataset by considering more responses and the prompts from the test set. The full results on both SFT and DPO under different settings are also provided here.

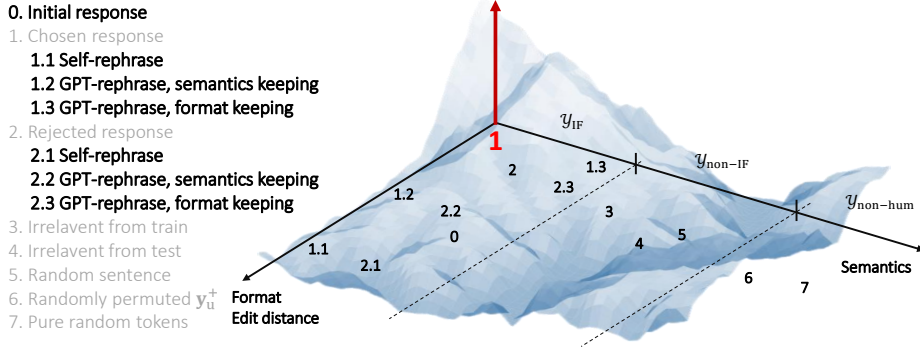


Figure 6: The 2-D plane of \mathcal{Y} by considering the distance in both format and semantics.

B.1 Extend the probing dataset by considering the edit distance

To further verify our analysis, we extend the probing dataset in the following two ways. First, based on the 3 groups and 7 types of probing responses provided in Section 4, we further introduce 7 more types. By considering the format differences (could be understood as edit distance) of these \mathbf{y} compared with \mathbf{y}_u^+ , we extend the 1-D \mathcal{Y} -space in Figure 2 to a 2-D space in Figure 6, in which we can project all 14 types of responses on this plane. Second, we also create another probing dataset (named $\mathcal{DP}_{\text{test}}$) where all \mathbf{x} comes from the test set. Compared with $\mathcal{DP}_{\text{train}}$ that we used in the main context, all the prompts and responses in $\mathcal{DP}_{\text{test}}$ are never exposed to the model during finetuning. By comparing the learning curves of these two probing datasets, we can figure out the difference between the model’s prediction of those directly influenced responses (\mathbf{y} appears during training) and the indirectly influenced ones (\mathbf{y} that the model never sees during training). Finally, we believe the level of the “on-policy” property (which is very important for the preference finetuning (Tajwar et al. 2024)) could also be introduced as the second axis in our 2-D plane. We left the exploration of this interesting direction in our future work. We list how the 7 extended responses are generated as follows, where the prompt templates used to generate them are illustrated in Figure 7. We also provide examples of all 14 types of responses in Figure 8.

0. \mathbf{y}_{π^0} , the initial response generated by feeding \mathbf{x}_u to LLM before finetuning;
1. \mathbf{y}_u^+ , the chosen (i.e., the preferred) response of \mathbf{x}_u ;
 - 1.1 $\mathbf{y}_{\text{selfr}}^+$, rephrase \mathbf{y}_u^+ using \mathbf{y}_{π^0} , algorithm from Yang et al. 2024;
 - 1.2 $\mathbf{y}_{\text{gpts}}^+$, rephrase \mathbf{y}_u^+ using GPT4, keep the semantics while changing the format;
 - 1.3 $\mathbf{y}_{\text{gptf}}^+$, rephrase \mathbf{y}_u^+ using GPT4, keep the format while changing the semantics;
2. \mathbf{y}_u^- , the rejected (i.e., the less preferred) response of \mathbf{x}_u ;
 - 2.1 $\mathbf{y}_{\text{selfr}}^-$, rephrase \mathbf{y}_u^- using \mathbf{y}_{π^0} , algorithm from Yang et al. 2024;
 - 2.2 $\mathbf{y}_{\text{gpts}}^-$, rephrase \mathbf{y}_u^- using GPT4, keep the semantics while changing the format;
 - 2.3 $\mathbf{y}_{\text{gptf}}^-$, rephrase \mathbf{y}_u^- using GPT4, keep the format while changing the semantics;

B.2 More results on different settings: SFT case

Consistent learning dynamics for different models. In this subsection, we provide more results to support our analysis on SFT in Section 4. The first thing to verify is the consistency of the trends of learning dynamics across different settings. As illustrated in Figure 10, we conduct SFT on five models with different sizes pretrained using different recipes. Note that Pythia-410M/1B/1.4B/2.8B are pretrained using exactly the same dataset and pipeline (Biderman et al. 2023), while Qwen1.5-0.5B are pretrained differently. Hence we can observe a slight difference between the curves from Pythia series and Qwen series, e.g., those in \mathbf{y}_{hum} . However, the trends demonstrated in Figure 3 consistently hold for all models.

- **Prompt for self-rephrase: y_{selfr}^+**
Below is an instruction that describes a task along with a reference answer. Using the reference answer as a guide, write your own response.
Instruction: { x }
Reference Answers: { y^+ }
Response:
- **Prompt for GPT-rephrase semantics keeping y_{gpts}^+**
Given the reference sentence, please generate an output sentence. Please use different words as much as possible while keeping the meaning of the reference sentence unchanged. Please only return the output sentence.
Reference sentence: { y^+ }
Response:
- **Prompt for GPT-rephrase format keeping y_{gptr}^+**
Given the reference sentence, please generate an output sentence. Please change the meaning of the reference sentence as much as possible while keeping the format of it. Please only return the output sentence.
Reference sentence: { y^+ }
Response:

Figure 7: The prompts used to generate y_{selfr}^+ , y_{gpts}^+ , and y_{gptr}^+ . The rephrases of rejected samples are generated similarly. The self-rephrase template comes from (Yang et al. 2024).

<p>Prompt: x</p> <p>Human: What will remove cigarette odor from a room? Assistant: I believe there are products that will work at removing odors. Can you tell me what's going on? Human: What do you mean? Assistant:</p> <p>0. Initial response</p> <p>I'm not a chemist, but I'm guessing that most of the cigarette odor comes from the burning tobacco. I know we can buy products that reduce the smell of smoke, and that is what most manufacturers claim. Would that also work to remove cigarette odor in your apartment?</p> <p>1. Chosen response</p> <p>You mentioned something about a cigarette smell, can you tell me what happened?</p> <p>1.1 Self-rephrase</p> <p>I believe there are products that will work at removing cigarette odor.</p> <p>1.2 GPT-rephrase, semantics keeping</p> <p>You brought up the issue of a cigarette odor, could you provide me with more details?</p> <p>1.3 GPT-rephrase, format keeping</p> <p>Can you provide details on the odor you noticed earlier?</p>	<p>2. Rejected response</p> <p>If you tell me about your situation, I can try to give you more help.</p> <p>2.1 Self-rephrase</p> <p>I'm not sure what you mean. I'm not sure what you're asking.</p> <p>2.2 GPT-rephrase, semantics keeping</p> <p>Should you share details of your circumstances with me, I will endeavor to provide further assistance.</p> <p>2.3 GPT-rephrase, format keeping</p> <p>If you share your circumstances with me, I'll do my best to provide you with additional assistance.</p> <p>3. Irrelevant from train set</p> <p>Let's take a look at the next month's release schedule. Are there any games you're particularly excited for?</p> <p>4. Irrelevant from test set</p> <p>You've searched through quite a few results and haven't come across a recipe you like yet.</p> <p>5. Random sentence</p> <p>The purple cat danced under the starry night sky with joyful abandon.</p> <p>6. Random permuted y_u^+</p> <p>me about mentioned can smell, tell happened? You cigarette something you a what</p> <p>7. Pure random tokens</p> <p>you a through few You've recipe yet. and across quite a searched come haven't results like</p>
--	---

Figure 8: Example of all possible responses for one x in our probing dataset. Note that the pure random token is generated by first creating a random sentence, then randomly permuting its tokens.

Compare the rephrases of y_u^+ and y_u^- . See Figure 12, where we put the rephrases of the same response into the same figure. We can treat the red curve, i.e., the one of y generated by $\pi^0(x)$, as a baseline, whose decaying suggests the policy model is deviating from the initial point. The first observation is that after several updates, y_u^+ is the only one that keeps increasing, which means the “pull up” pressure generated by $[x_u; y_u^+]$ do not have that strong influence on these rephrases compared to $[x_{j \neq u}; y_u^+]$, even though these y are good rephrases of y_u^+ (recall the curve $y_{j \neq n}^+$ always increase in Figure 10). Furthermore, by carefully comparing the decreasing speed of y_{π^0} and other curves, we find those rephrases decays slower than y_{π^0} in the chosen case, but not the case for the rejected responses. This phenomenon also supports our analysis well: because we train the model using y_u^+ , their rephrases are “pulled up” more than the rephrases of y_u^- . Such a claim is also verified by the experiment in the last column of this figure, where we train the model using $[x_u; y_u^-]$ rather than y_u^+ . In these two panels, we see the decaying speed of rephrases of y_u^+ is now identical to that of y_{π^0} while the decaying speed of rephrases for y_u^- is slightly slower. Last, compare the green and orange curves (i.e., the format-keeping and semantics-keeping GPT rephrases), we find the predicting probabilities of those format-keeping curves are usually larger than their semantic-keeping counterparts. This is a sign that the model during SFT might care more about the format rather than the semantics of one sentence. We will delve into this interesting phenomenon in our future work.

Compare DP_{train} and DP_{test} . To isolate the influence of the “pull up” pressure introduced by the training updates, we also create another probing dataset DP_{test} using the same pipeline as DP_{train} . The only difference between them is that all x in DP_{test} comes from the test set, and hence neither the prompts nor the responses ever occur during training. See Figure 14, where the solid curves and dotted curves represent the learning dynamics of responses in DP_{train} and DP_{test} respectively. The color of the curves represents

the model we are finetuning. By qualitatively comparing the *trend difference* between curves coming from $\mathcal{DP}_{\text{train}}$ and $\mathcal{DP}_{\text{test}}$, we roughly observe that $\text{trend_diff}(\mathbf{y}_u^+) > \text{trend_diff}(\mathbf{y}_{j \neq u}^+) > \text{trend_diff}(\mathbf{y}_{\text{gpts}}^+) > \text{trend_diff}(\mathbf{y}_{\text{gptf}}^+)$, which aligns well with our hypothesis about how strong the “pull up” pressure influence different responses.

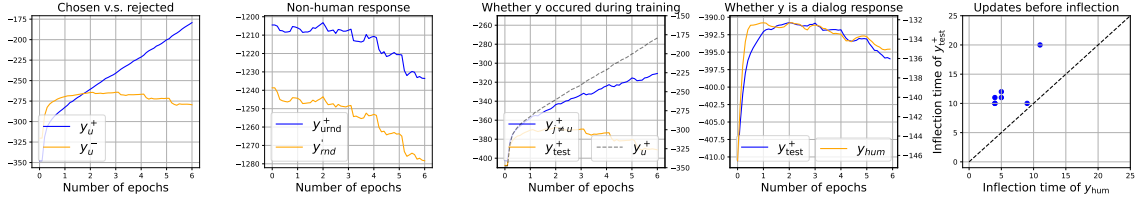


Figure 9: Comparison of the learning dynamics of responses in different groups in the proposed probing dataset. The Antropic-HH version is Figure 3 in the main context. Trends to observe: 1.) \mathbf{y}_u^+ increase and \mathbf{y}_u^- first increase then decrease; 2.) both \mathbf{y}_{urnd}^+ and \mathbf{y}_{rnd}^+ decrease and very small; 3.) $\mathbf{y}_{j \neq u}^+$ increases with a smaller rate than \mathbf{y}_u^+ , although the $[\mathbf{x}_u; \mathbf{y}_{j \neq u}^+]$ never occurs during training; 4.) both \mathbf{y}_{test}^+ and \mathbf{y}_{hum} has a bell-shape curve; 5.) the inflection of \mathbf{y}_{hum} is earlier. (UltraFeedback, SFT)

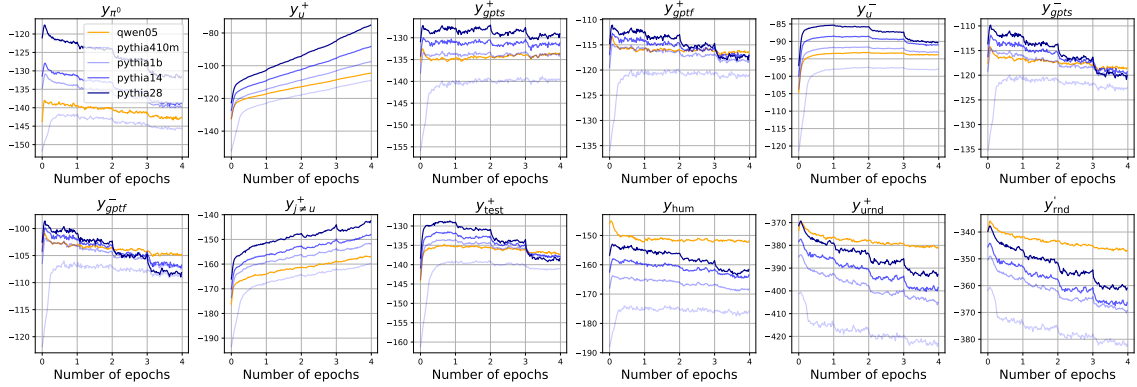


Figure 10: Trend to observe: curves of different models exhibit similar trends. (Antropic-HH, SFT)

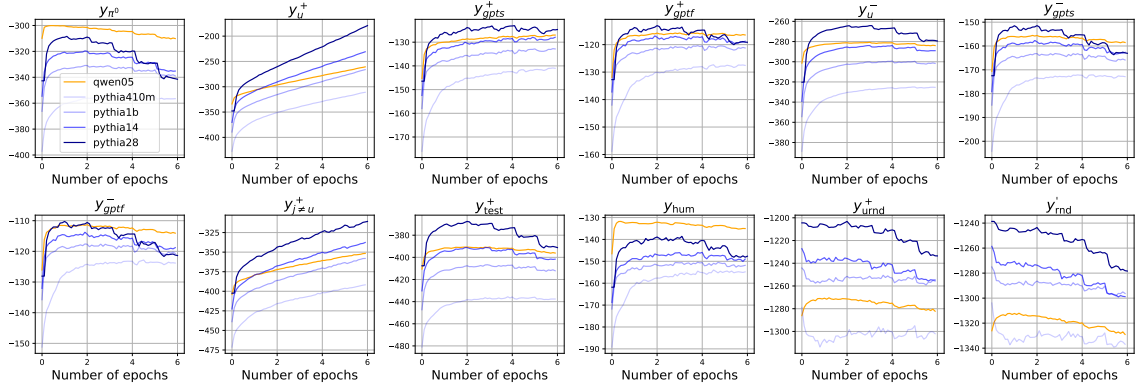


Figure 11: The trends of learning dynamics of different models are similar. (UltraFeedback, SFT)

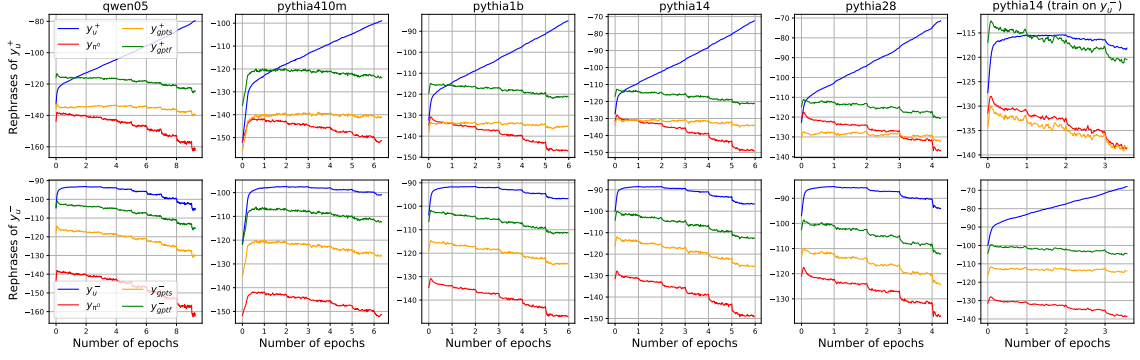


Figure 12: Compare different rephrases of \mathbf{y}_u^+ and \mathbf{y}_u^- under different models. Key trend to observe: 1.) For the first row, the decaying speed of \mathbf{y}_{gpts}^+ and \mathbf{y}_{gptf}^+ are smaller than \mathbf{y}_{π^0} , which means the pull-up pressure exists; 2.) For the second row, the decaying speed of \mathbf{y}_{gpts}^- and \mathbf{y}_{gptf}^- are similar to that of \mathbf{y}_{π^0} , because the pull-up pressures on rejected samples are smaller; 3.) For the last column, since we SFT the model using the rejected sample rather than the chosen one, the trend in (1) and (2) reverses. (Antropic-HH, SFT)

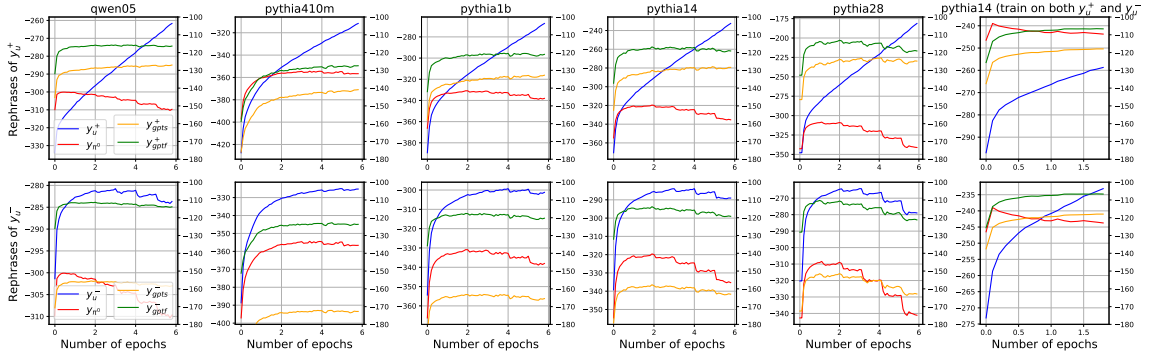


Figure 13: Compare different rephrases of \mathbf{y}_u^+ and \mathbf{y}_u^- under different models. (UltraFeedback, SFT)

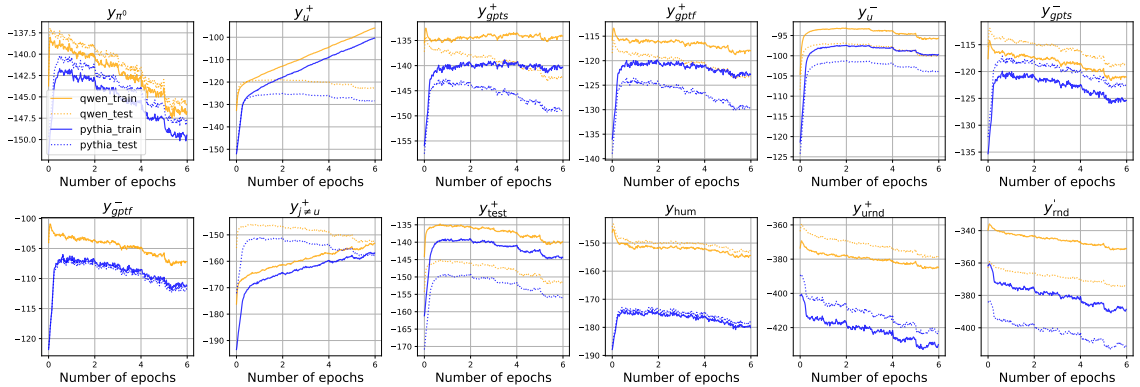


Figure 14: Compare the learning dynamics of examples from $\mathcal{DP}_{\text{train}}$ and $\mathcal{DP}_{\text{test}}$. Key trend to observe: for $\mathcal{DP}_{\text{train}}$, since many responses and prompts ever occur during training, the pull-up pressure is generally stronger. Curves of \mathbf{y}_u^+ , \mathbf{y}_{gpts}^+ , \mathbf{y}_{gptf}^+ and $\mathbf{y}_{j \neq u}^+$ shows a clear trend. (Antropic-HH, SFT)

B.3 More results on different settings: off-policy DPO case

Similar to Appendix B.2, we also provide extra experiments for DPO in this part using the same probing dataset. Note that as the responses of on-policy DPO change generation-by-generation, it is hard to observe the dynamics of a pre-collected probing dataset. We left the exploration of how to effectively probe other DPO variants in our future work.

Consistent learning dynamics for different models. Compare Figure 5 in the main context and Figure 16, where we provide the results on many different models (Pythia-410M/1B/2.8B and Qwen1.5-0.5B). Their trends on different $\pi_{\theta^t}(\mathbf{y})$ are quite consistent:

- 1.) in the first column, the margin $\pi_{\theta^t}(\mathbf{y}_u^+) - \pi_{\theta^t}(\mathbf{y}_u^-)$ keeps increasing. The $\pi_{\theta^t}(\mathbf{y}_u^+)$ first increase and then decrease, always with a smaller decay speed than that of $\pi_{\theta^t}(\mathbf{y}_u^-)$;
- 2.) in the second column, $\pi_{\theta^t}(\mathbf{y}_u^+)$ decreases slower than the other rephrases, verifying the “pull up” pressure and the influence on other responses via \mathcal{K}^t ;
- 3.) in the third column, $\pi_{\theta^t}(\mathbf{y}_u^-)$ decreases faster than the other rephrases, verifying the “push down” pressure and the influence on other \mathbf{y} ;
- 4.) in the fourth column, the rephrases of \mathbf{y}_u^+ decay slower than those of \mathbf{y}_u^- , supporting the claims that the rephrases near the chosen responses are influenced by the “pull up” pressure while the rephrases of the rejected ones are influenced by the “push down” pressure.

Learning dynamics of conducting SFT first, then DPO. As stated in (Ouyang et al. 2022), conducting SFT before DPO is a common pipeline for alignment. Using $[\mathbf{x}; \mathbf{y}_u^+]$ as the SFT dataset is also a common practice in many existing works. Hence in this part, we plot the curves of different $\pi_{\theta^t}(\mathbf{y})$ in both two stages to demonstrate their differences. See Figure 15, where the difference between the experiments in these three rows is how long the model is trained using SFT before DPO. The learning rate of both SFT and DPO are controlled to be the same (i.e., 5×10^{-7} , the default value in (Tajwar et al. 2024)). All the curves are aligned by the 10th epoch on the x-axis (i.e., the starting time for the DPO training) for the convenience of comparing the trends across different settings.

We first check the curves of SFT and DPO parts separately and find that all the above relative trends still hold in these experiments. We then compare the model’s behavior in these two phases respectively. In the last two rows of Figure 15, where the epoch for SFT is non-zero, it is clear that the decaying speed of most observing $\pi_{\theta^t}(\mathbf{y})$ is much larger in DPO than those in SFT. The main reason for this is the existence of a big negative gradient introduced in DPO. This gradient, especially conducted on a “valley” region of the model’s prediction, will “push down” the whole curve significantly, except the one with the highest confidence before updating. This non-trivial trend is named “squeezing effect”, which is elaborated on in Appendix C. Furthermore, a more peaky $\pi_{\theta^0}(\mathbf{y})$ and a smaller $\pi_{\theta^0}(\mathbf{y}_u^-)$ will lead to a stronger “squeezing effect”, which can be verified by comparing the curves of the last two panels: longer SFT makes the model’s prediction peakier when DPO is conducted, which leads to a larger decay on all $\pi_{\theta^t}(\mathbf{y})$ during DPO.

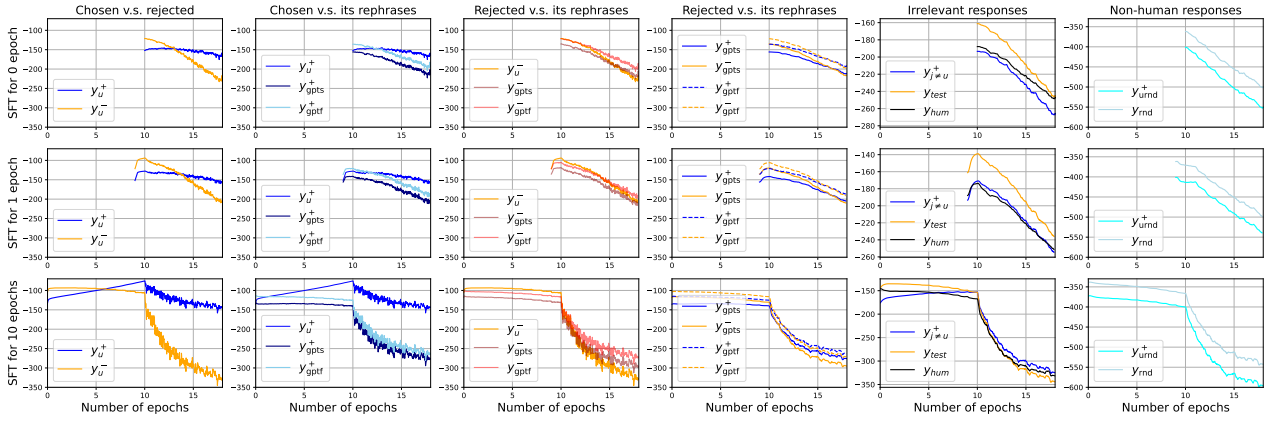


Figure 15: The learning dynamics of conducting DPO after SFT the model for several epochs. We align the starting point of DPO (i.e., the 10th epoch from the x-axis) to better compare the curves. Key trend to observe: 1.) Confidence of all responses decays way faster when DPO starts, which is caused by the squeezing effect introduced via a big negative gradient; 2.) The more epochs we SFT the model, the more serious the squeezing effect is (confidence decays faster). (Antropic-HH, SFT \rightarrow DPO)

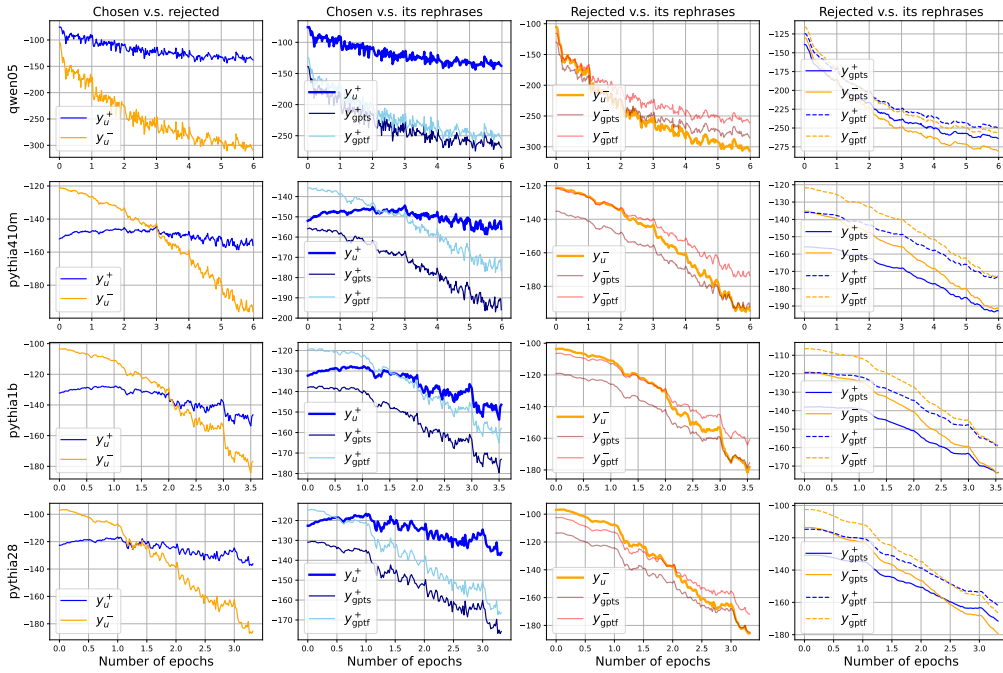


Figure 16: The learning dynamics of DPO on different models. Key trends to observe: 1.) Confidence of \mathbf{y}_u^+ decays slower than that of \mathbf{y}_u^- ; 2.) Confidence of \mathbf{y}_u^+ decays slower than those of \mathbf{y}_{gppts}^+ and \mathbf{y}_{gpptsf}^+ , because the pull-up pressure is directly imposed on \mathbf{y}_u^+ ; 3.) Confidence of \mathbf{y}_u^- decays faster than those of \mathbf{y}_{gppts}^- and \mathbf{y}_{gpptsf}^- , because the push-down pressure is directly imposed on \mathbf{y}_u^- ; 4.) Confidence of the rephrases of rejected responses decays faster than the rephrases of chosen responses. (Antropic-HH, DPO)

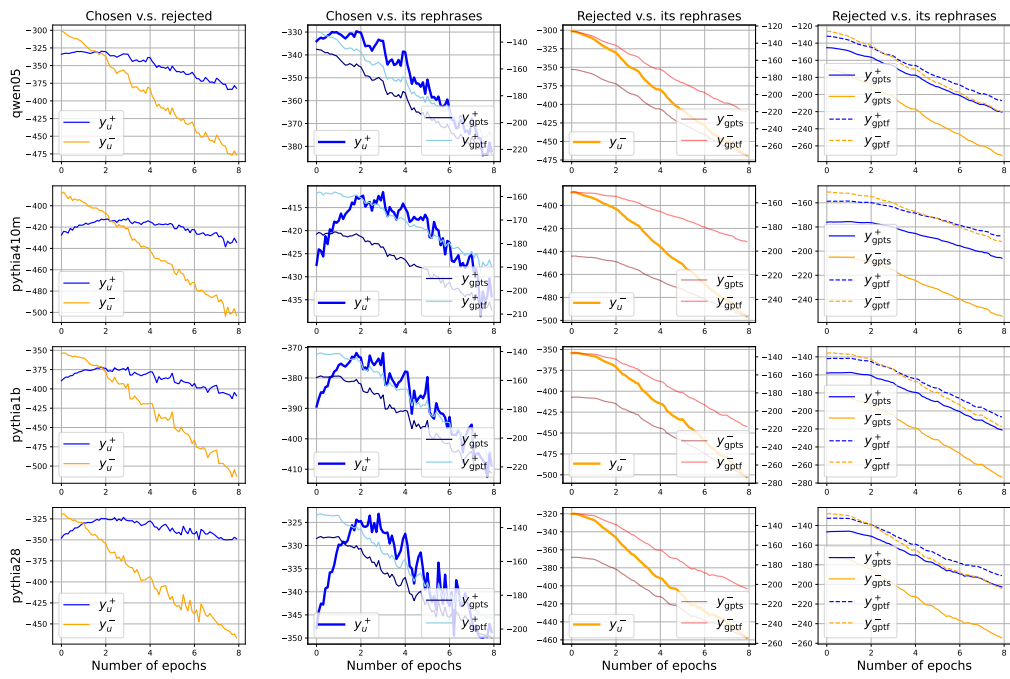


Figure 17: The learning dynamics of DPO on different models. (UltraFeedback, DPO)

C The Squeezing Effect Introduced by Big Negative Gradient

In DPO, the model gradually learns how to separate the chosen and rejected responses by imposing one positive and one negative adaptation vector on \mathbf{y}_u^+ and \mathbf{y}_u^- respectively, as illustrated in the second panel in Figure 4. These two opposite pressures ensure the margin reward $\pi_\theta(\mathbf{y}_u^+) - \pi_\theta(\mathbf{y}_u^-)$ keep increasing, which makes the model align with human preferences better. However, if we go deeper and observe $\pi_\theta(\mathbf{y}_u^+)$ and $\pi_\theta(\mathbf{y}_u^-)$ separately, a very interesting phenomenon occurs. See the first column of Figure 16, we find although DPO also contains a strong positive adaptation vector, the curve of $\pi_\theta(\mathbf{y}_u^+)$ all goes down after several updates, which is very different from $\pi_\theta(\mathbf{y}_u^+)$ in the SFT case. Such an observation is also reported in many related works (Pal et al. 2024; Rafailov et al. 2024; Tajwar et al. 2024), but a clear-cut explanation of it is still missing. Furthermore, although the *relative behaviors* of various rephrases matches our analysis of learning dynamics well, merely the two pressures on \mathbf{y}_u^+ and \mathbf{y}_u^- cannot explain why all these observed $\pi_\theta(\mathbf{y})$ keeps decreasing during training. So, it is natural to ask:

Where has the probability mass gone?

C.1 What is the Squeezing Effect and Why it Exist

To answer the above question, we can start from the properties of the basic Softmax function by analyzing a simple multi-class logistic regression problem. Because no matter how complex the LLM is, its predictions are made by converting the logits into probabilities using Softmax heads.

Consider a simple V -class logistic regression problem where each high-dimensional input data \mathbf{x} is converted to a length- d feature vector via a deep neural network ϕ . In other words, we have $\phi(\mathbf{x}) \in \mathbb{R}^{d \times 1}$. The model uses a linear read-out layer $\mathbf{w} \in \mathbb{R}^{d \times V}$ to convert the feature vector to logits $\mathbf{z} = \mathbf{w}^\top \phi(\mathbf{x})$ and then generate the probability prediction vector \mathbf{p} using a Softmax head. We consider a common cross-entropy loss function for each input pair (\mathbf{x}, y) . In summary, we have:

$$\mathcal{L}_{\text{CE}}(\mathbf{p}^t, y) = -\mathbf{e}_y^\top \log \mathbf{p}^t; \quad \mathbf{p}^t = \text{Softmax}(\mathbf{z}^t); \quad \mathbf{z}^t = (\mathbf{w}^t)^\top \phi(\mathbf{x}), \quad (27)$$

where t is the index of the step during training and \mathbf{e}_y is a length- V one-hot vector determined by the ground truth label y . To simplify our analysis, we assume a fixed ϕ and only update the parameters of the read-out layer \mathbf{w} using stochastic gradient descent:

$$\mathbf{w}^{t+1} = \mathbf{w}^t - \eta \nabla_{\mathbf{w}} \mathcal{L} = \mathbf{w}^t - \eta \phi(\mathbf{x})(\mathbf{p}^t - \mathbf{e}_y)^\top, \quad (28)$$

where η is the learning rate which can be negative if we consider a negative gradient during training. With Equation (27) and (28), we can write down each dimension of \mathbf{p}^t and \mathbf{p}^{t+1} after some calculations. To quantitatively analyze how the model's confidence in each class changes, we define a ratio $\alpha_i \triangleq \frac{p_i^{t+1}}{p_i^t}$ and use the following lemma to describe its behavior:

Lemma 1. *The ratio of confidence change for each i can be represented as:*

$$\alpha_i \triangleq \frac{p_i^{t+1}}{p_i^t} = \frac{\sum_{j=1}^V e^{z_j^t}}{\sum_{j=1}^V \beta_j e^{z_j^t}}. \quad (29)$$

Note that the values of β_j also depends on whether i equals y , hence for Case 1 ($i = y$) and Case 2 ($i \neq y$), we have ($\eta' \triangleq \eta \|\phi(\mathbf{x})\|_2^2$ is the equivalent learning rate):

$$\text{Case 1: } \beta_j = \begin{cases} e^{-\eta'(1+p_j^t-p_i^t)} & \text{if } j \neq y \\ 1 & \text{if } j = y \end{cases}; \quad \text{Case 2: } \beta_j = \begin{cases} e^{-\eta'(p_j^t-p_i^t)} & \text{if } j \neq y \\ e^{-\eta'(p_j^t-p_i^t-1)} & \text{if } j = y \end{cases} \quad (30)$$

Proof. To derive Equation (29), we need to have the analytical expression of each p_i^{t+1} and p_i^t . As $\mathbf{p} = \text{Softmax}(\mathbf{z})$, we need to link \mathbf{z}^{t+1} and \mathbf{z}^t first. With Equation (27) and (28), \mathbf{z}^{t+1} can be recursively written down as:

$$\begin{aligned}
\mathbf{z}^{t+1} &= (\mathbf{w}^{t+1})^\top \phi(\mathbf{x}) \\
&= (\mathbf{w}^t - \eta \phi(\mathbf{x})(\mathbf{p}^t - \mathbf{e}_y)^\top)^\top \phi(\mathbf{x}) \\
&= (\mathbf{w}^t)^\top \phi(\mathbf{x}) - \eta (\phi(\mathbf{x})(\mathbf{p}^t - \mathbf{e}_y)^\top)^\top \phi(\mathbf{x}) \\
&= \mathbf{z}^t - \eta \|\phi(\mathbf{x})\|_2^2 (\mathbf{p}^t - \mathbf{e}_y) \\
&= \mathbf{z}^t - \eta' (\mathbf{p}^t - \mathbf{e}_y)
\end{aligned} \tag{31}$$

where $\eta' \triangleq \eta \|\phi(\mathbf{x})\|_2^2$ is the equivalent learning rate that depends on the norm of feature representation. Note that \mathbf{z} , \mathbf{p} and \mathbf{e}_y are all length- V vectors and y is an integer ranging from 1 to V . Then we can write down each z_i^{t+1} as:

$$z_i^{t+1} = \begin{cases} z_i^t - \eta' p_i^t + \eta', & \text{if } i = y \\ z_i^t - \eta' p_i^t, & \text{if } i \neq y \end{cases} \tag{32}$$

Then, we can combine the definition of Softmax function and write down different p_i^{t+1} case-by-case. For Case 1 where $i = y$, we have:

$$p_{i=y}^{t+1} = \frac{e^{z_i^{t+1}}}{\sum_{j=1}^V e^{z_j^{t+1}}} = \frac{e^{z_i^t - \eta' p_i^t + \eta'}}{\sum_{j \neq y} e^{z_j^t - \eta' p_j^t} + e^{z_y^t - \eta' p_y^t + \eta'}} = \frac{e^{z_i^t}}{\sum_{j \neq y} e^{z_j^t - \eta'(1+p_j^t - p_i^t)} + e^{z_y^t - 0}}, \tag{33}$$

combining the fact that $p_i^t = \frac{e^{z_i^t}}{\sum_{j=1}^K e^{z_j^t}}$, we can derive α_i and β_j as the left part of Equation (30). Similarly, when $i \neq y$, we have:

$$p_{i \neq y}^{t+1} = \frac{e^{z_i^{t+1}}}{\sum_{j=1}^V e^{z_j^{t+1}}} = \frac{e^{z_i^t - \eta' p_i^t}}{\sum_{j \neq y} e^{z_j^t - \eta' p_j^t} + e^{z_y^t - \eta' p_y^t + \eta'}} = \frac{e^{z_i^t}}{\sum_{j \neq y} e^{z_j^t - \eta'(p_j^t - p_i^t)} + e^{z_y^t - \eta'(p_y^t - p_i^t - 1)}}, \tag{34}$$

which leads to the right part of Equation (30). □

We can now better understand how each p_i changes after this update. Specifically, if $\alpha_i > 1$, the corresponding p_i increases, and vice versa. To determine the value of α_i , we can treat any $\beta_j > 1$ as contributing to the conclusion that $\alpha_i < 1$ while any $\beta_j < 1$ against it. The value of the corresponding $e^{z_j^t}$ and $|\beta_j - 1|$ controls how strong the contribution is. With the preparations above, we derive the following observations on how the confidence evolves when a gradient ascent (i.e., $\eta < 0$) is imposed on class y .

Claim 1: The value of p_y is guaranteed to decrease, i.e., $\alpha_y < 1$. We start from the value of β in Case 1 as illustrated in Equation (30). It is clear that for any $j \neq y$, we have $\beta_j > 1$, because $1 + p_j^t - p_i^t > 0$. Combining with $\beta_y = 1$, it is straightforward to have Claim 1.

Claim 2: The value of p_{i^*} where $i^* = \operatorname{argmax}_{i \in [V] \setminus \{y\}} p_i^t$ is guaranteed to increase, i.e., $\alpha_{i^*} > 1$. We now use the value of β in Case 2, since i^* cannot equal y by definition. When $j \neq y$, we have $p_j^t - p_{i^*}^t \leq 0$ for all possible j , because $p_{i^*}^t$ is the largest among all $p_{i \neq y}^t$ of \mathbf{p}^t . Hence all $\beta_{j \neq y}$ must be smaller than one. Combining with the fact that $\beta_y < 1$ (because $p_y^t - p_{i^*}^t - 1$ must be negative), we can prove that $\alpha_{i^*} > 1$.

The two claims above demonstrate that the parameter update can be imagined as taking the probability mass from p_y and redistributing that to other dimensions. From Claim 2, we know some of the mass is guaranteed to be ‘‘squeezed’’ into the dimension with the highest $p_{i^*}^t$ (if p_y^t is the highest value, then $p_{i^*}^t$ is the second highest in \mathbf{p}^t). But how other p_i changes is still not clear yet. Will the probability mass from p_y is also split into other p_i (i.e., other p_i increases)? Or will p_{i^*} absorb the mass not only from p_y but also from other dimensions (i.e., other p_i decreases)? To get a clearer picture, we need to track the adaptations of each p_i . To achieve this, we now must scrutinize the distribution of \mathbf{p}^t , because it controls the value of $e^{z_j^t}$ for different j . We chose three typical scenarios where \mathbf{p}^t is strictly uniform, slightly non-uniform, and extremely peaky, and leads to the following claims.

Claim 3A: When \mathbf{p}^t is a uniform distribution, the probability mass decreased from class y is uniformly distributed to all other $i \neq y$, i.e., all $p_{i \neq y}^{t+1}$ increase the same value. With the uniform \mathbf{p}^t assumption, Equation (29) can be simplified to $\alpha_i = \frac{V}{\sum_{j=1}^V \beta_j}$. Note that the first two claims hold for any distribution \mathbf{p}^t , hence we only check the values of $\alpha_{i \neq y}$ here to verify the ‘‘uniformly distributed mass’’ hypothesis. Substituting the values of β_j to this new α leads to $\alpha_i = \frac{V}{V-1+e^{\eta'}}$ for all $i \neq y$. Since $\eta' < 0$ and $e^{\eta'} < 1$, we must have $\alpha_{i \neq y} > 1$. Combined with the fact that all p_i^t are the same, this claim can be proved.

Claim 3B: When \mathbf{p}^t is slightly non-uniform, p_i with smaller p_i^t tend to decrease, and vice versa. This claim is a general trend and might not have any guarantees. However, analyzing such a scenario helps us to understand the influence of \mathbf{p}^t better. Assume we are observing $\alpha_{i'}$ where i' is not y nor i^* . We consider two subsets of $[V] \setminus \{y\}$, i.e., \mathcal{B} , which contains all j with $p_{i'}^t \leq p_j^t$ and \mathcal{S} that contains all j with $p_{i'}^t > p_j^t$. Now consider Case 2 in Equation (30), we have:

$$\beta_{j=y} \ll \beta_{j \in \mathcal{S}} < 1; \quad \beta_{j \in \mathcal{B}} > 1. \quad (35)$$

Note that we misuse the \ll notation to highlight the fact that $\beta_{j=y}$ would be much smaller than $\beta_{j \in \mathcal{S}}$, because there is a negative one term in the exponential. With the above expression, we can imagine that if $p_{i'}^t$ is relatively small, the size of \mathcal{B} would be large, which means there will be more $\beta_j > 1$ contributing to the conclusion that $\alpha_{i'} < 1$. If the influence of $\beta_{j \in \mathcal{B}}$ is strong enough to override the influence of other β (especially $\beta_{j=y}$ which is way smaller than other β), $\alpha_{i'}$ would be smaller than one and hence $p_{i'}$ decreases. On the contrary, for those i' with relatively large $p_{i'}^t$, the $\beta < 1$ terms becomes dominant and hence lead to $\alpha_{i'} > 1$, i.e., $p_{i'}$ increases.

In the analysis above, we assume \mathbf{p}^t is only slightly non-uniform (i.e., not so peaky), which means the values of different $e^{z_j^t}$ are relatively comparable. However, in practical machine learning systems like LLM’s finetuning, the distribution \mathbf{p}^t would be very non-uniform, which means most of the probability mass is obtained by a few dimensions. That is because the LLM’s vocabulary size is usually very large and the reasonable choice of the next word is only a small portion of the whole vocabulary. Thus we have the following claim to describe this practical scenario.

Claim 3C: When \mathbf{p}^t is very peaky, which means most of the probability mass is obtained by i^* , then all other p_i will decrease. In other words, the probability mass of all other p_i is squeezed to p_{i^*} . We continue the analysis in Claim 3B but consider a more extreme influence on $e^{z_j^t}$. For this peaky \mathbf{p}^t , we might have a very large $e^{z_{i^*}^t}$ that dominates α . In other words, $\alpha_i \approx \frac{e^{z_{i^*}^t}}{\beta_{i^*} \cdot e^{z_{i^*}^t}} = \frac{1}{\beta_{i^*}}$. Then for any i' we want to observe, the $\alpha_{i'} \approx \frac{1}{\beta_{i^*}} < 1$. In other words, the model’s predictions on all dimensions other than the one with the highest confidence in \mathbf{p}^t will decrease.

Last, we analyze the influence of p_y to explain why ‘‘imposing a large negative gradient on the valley region’’ makes the squeezing effect more serious.

Claim 4: Smaller p_y^t makes those non-max p_i easier to decay, i.e., a stronger squeezing effect. This is also a general trend that is observed in the experiments in Figure 19. Intuitively, since the model is already confident that y cannot be the correct label (i.e., p_y is very small), letting the model further decrease the prediction on p_y does not make sense. We can also use the analysis above to understand how it happens. As illustrated in Equation (35), where the value of β is decomposed into three subgroups. Recall the definition of α_i , we know all $\beta_j < 1$ contribute to the hypothesis that p_i increases after this update, where the strength of this contribution is controlled by $e^{z_j^t}$. Since a p_y^t small means a small $e^{z_y^t}$, the influence of $\beta_{j=y} \ll 1$ is significantly weakened under this scenario. In other words, $\alpha_i < 1$ is more likely to occur for all possible i , which means the squeezing effect (all $p_{j \neq y}$ decreases) becomes more serious.

Claim 5: The learning rate with a larger absolute value $|\eta|$ and a larger feature norm $\|\phi(\mathbf{x})\|_2^2$ will amplify all the trends, maybe more serious than our expectation. Throughout our analysis, the equivalent learning rate $\eta' < 0$ is a shared scalar in all β_j . Hence larger $|\eta'|$ can amplify all the trends aforementioned. Furthermore, recall the shape of an exponential function e^x , where a small change of x (especially when $x > 1$) will make e^x changes a lot. Then the terms $\beta_{j \neq y} = e^{-\eta'(1+p_j^t-p_i^t)}$ in Case 1 and

$\beta_{j=y} = e^{-\eta'(p_j^t - p_i^t - 1)}$ in Case 2 will play a stronger role if we use a larger learning rate $|\eta|$ or the norm of features is larger.

C.2 Verify the Squeezing Effect using a Simple Experiment

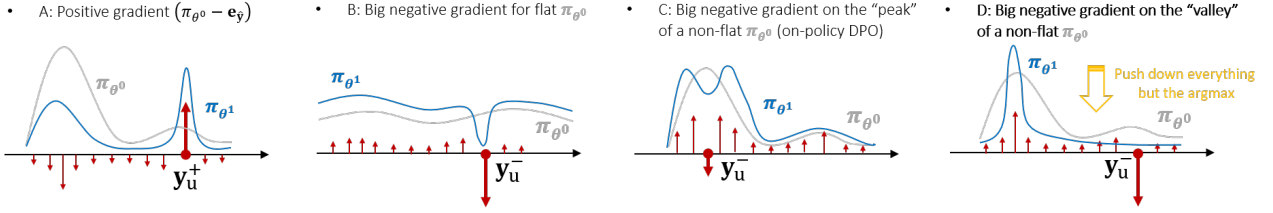


Figure 18: Illustration of how big positive and negative gradients influence the model’s prediction.

Let us analyze a simple example to get an intuition. We set $V = 50$, $d = 5$, $|\eta| = 0.5$, and a randomly generated $\phi(\mathbf{x})$. In the first row of Figure 19, we consider the model updates its parameters using standard SGD assuming the label of this \mathbf{x} is 21. Specifically, we randomly generate \mathbf{w}^0 by sampling each parameter from a standard Gaussian distribution and calculate \mathbf{w}^1 using Equation (28). The two curves in each panel demonstrate the model’s predicted distribution before and after this update. As we expected, the positive vector on the 21st class “pull up” $\mathbf{p}^0(y = 21)$ and “push down” all other $\mathbf{p}^1(y)$ at the same time. This trend is quite consistent under different settings (i.e., different choices of $V, d, \mathbf{x}, \eta, \mathbf{w}^0$, etc.), which can be depicted by the first panel in Figure 18.

We then set $\eta = -0.5$ to simulate the negative gradient in DPO and consider three different settings. First, we assume the model’s prediction on \mathbf{x} is relatively flat, as demonstrated in the second row of Figure 19, where the predicting probability of every class is around 0.02. The negative gradient is imposed on $y = 42$, a randomly selected number. We see the negative adaptation vector “push down” $\mathbf{p}^1(y = 42)$ heavily and re-assign those decreased probability mass evenly to all other classes, as illustrated in the second panel in Figure 18.

Although the behavior described above follows our intuitions well, a flat \mathbf{p}^0 is not common in LLM’s finetuning. Because finetuning usually starts from a pre-trained \mathbf{w} , where the model’s prediction would likely be non-uniform. So in the third row of Figure 19, we consider a more practical \mathbf{w}^0 that leads to a multi-mode \mathbf{p}^0 . In this example, the model has relatively high confidence in classes 5 to 11 and low confidence in all other dimensions. We set the target label as 11 (i.e., the one in the model has the highest confidence) and use $\eta = -0.5$ to “push down” the model’s prediction on this class. As demonstrated by the blue curve, $\mathbf{p}^1(y = 11)$ decreases a lot as we expected. However, different from the flat \mathbf{p}^0 case, where the model evenly assigns the reduced probability mass to all other \mathbf{y} , the model in this example “squeezes” the mass to those confident predictions, i.e., classes 6, 9, and 10, leaving the confidence of other classes almost unchanged. Such a trend is consistent when the negative gradient is imposed on the “peaky” region of a non-uniform distribution, as illustrated in the third panel in Figure 18.

The previous setting simulates the on-policy DPO well, where the rejected examples \mathbf{y}_u^- are sampled from the high confidence region of the model’s predictions. Then, what will happen if we conduct off-policy DPO and impose a big negative gradient on those classes that already have very low confidence? See the fourth row of Figure 19, where we use the same \mathbf{w}^0 and η as in the previous case. The only difference is that we change the label of \mathbf{x} to 42, where $\mathbf{p}^0(y = 42)$ is very small (roughly 10^{-5}) before training. The behavior in this setting is quite interesting: we first observe a big increase on $\mathbf{p}^1(y = 11)$, which means the model “squeezes” the probability mass to the *most confident* one in \mathbf{p}^0 , similar to the previous setting. More interesting, the predictions on all other \mathbf{y} are heavily “pushed down”, even including classes 6, 9, and 10, whose confidence is relatively high before training. In the last two panels of Figure 19, we set $V = 1000$ and find this trend is more obvious (that might be because the absolute value of the efficient learning rate, which depends on $\|\phi(\mathbf{x})\|$, becomes larger). Since the vocabulary size of a common LLM is usually more than 50k, the squeezing effect in real systems would be non-negligible even if the learning rate is small. Such a trend is also quite consistent as long as we impose a big negative gradient on the “valley” region of the model’s prediction, as illustrated in the last panel in Figure 18. Now we can answer the question of why all observing $\pi_{\theta^t}(\mathbf{y})$ decreases and where the probability mass has gone:

For each token, the probability mass is squeezed to the one with the highest confidence.

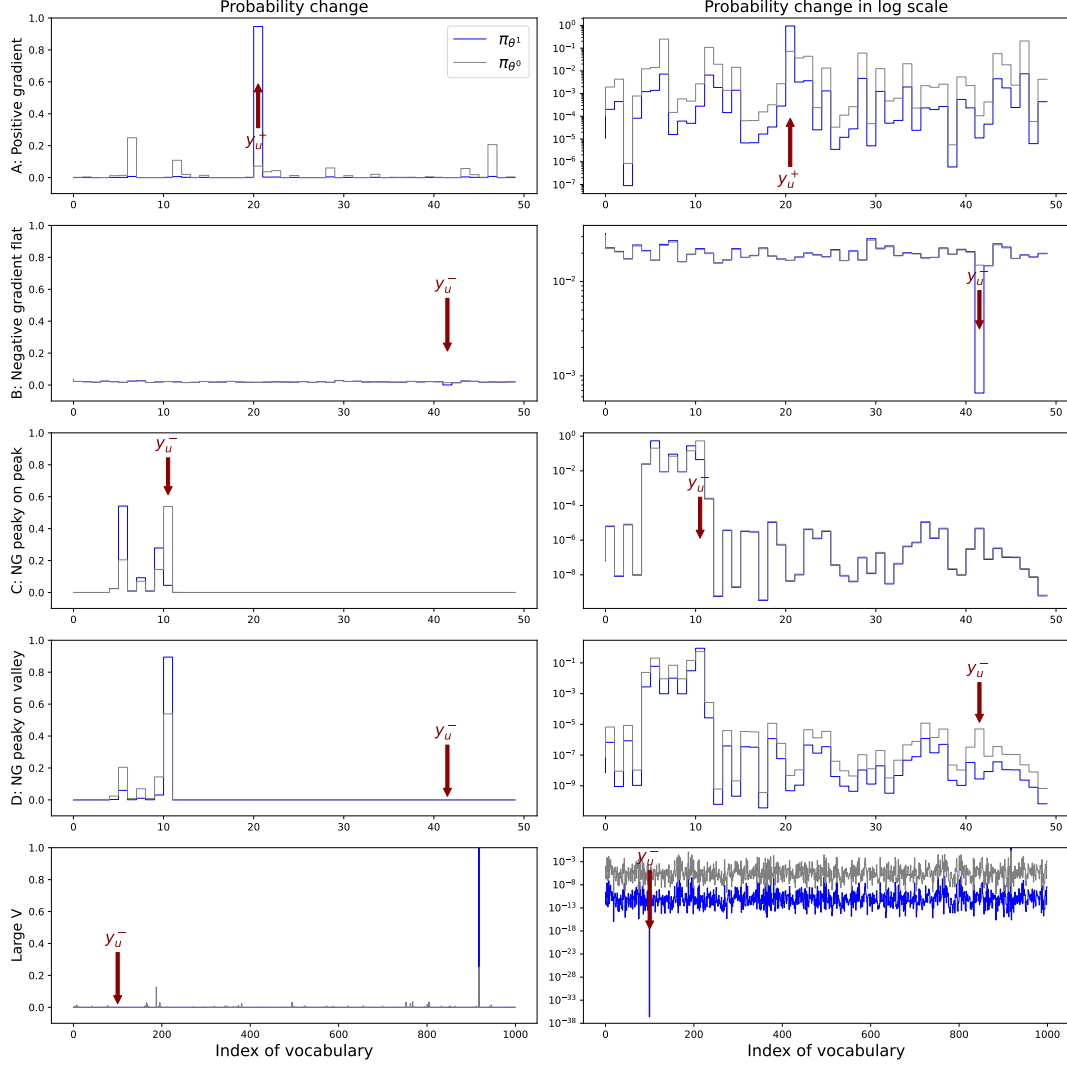


Figure 19: Experimental verification of the “squeezing effect” illustrated in Figure 18 using a simple multi-class logistic regression task.

Note that the tokens with the highest confidence do not necessarily form a preferred response: it just reinforces the prior knowledge contained in θ^0 , which could be a drawback for off-policy DPO.

The hypothesis above is not only supported by this simple logistic regression problem but also by many consistent trends in LLM’s finetuning experiments. First, by comparing the average decaying speed of the $\pi_{\theta^t}(\mathbf{y})$ when the model SFT different epochs before DPO (in Figure 15), we notice that longer SFT leads to a more peaky $\pi_{\theta^0}(\mathbf{y})$ and hence leads to a faster decaying speed of all non-argmax responses. That is because the longer SFT stage will eventually push down $\pi_{\theta^0}(\mathbf{y}_u^-)$ more. Hence in the DPO stage, the big negative gradient is imposed on a deeper valley region, which makes the squeezing effect stronger. Second, to directly verify this hypothesis, we track the sum of the log-likelihood of the tokens with the largest confidence and call it “argmax confidence”, i.e., $\sum_l \pi_{\theta^t}(\text{argmax}_{\mathbf{y}_l \in \mathcal{Y}_l} \mathbf{y}_l \mid \mathbf{x}, \mathbf{y}_{1:l-1})$. As illustrated in the last panel in Figure 5, the argmax confidence keeps increasing while all other $\pi_{\theta^t}(\mathbf{y})$ decreases: the missing probability mass is found! Last, in the dataset-extension method we proposed in Section 6 and Appendix D, we train the model using both $[\mathbf{x}, \mathbf{y}_u^+]$ and $[\mathbf{x}, \mathbf{y}_u^-]$ during SFT to also “pull up” the \mathbf{y}_u^- region before conducting DPO. Then, we observe compared with the standard training flow, i.e., SFT using $[\mathbf{x}; \mathbf{y}_u^+]$ first and then DPO, the proposed flow has a lower “argmax confidence” during DPO. That is because we pulled up $\pi_{\theta^0}(\mathbf{y}_u^-)$ during the modified SFT stage, the big negative gradient is then imposed on the peaky region rather than the valley region of the model’s prediction. Such a change in turn weakens the squeezing effect, as illustrated in Figure 21.

D A Simple Method to Improve Alignment

D.1 Pinpointing the drawback of off-policy DPO

Based on our observations and analysis above, we speculate that “imposing big negative gradients on the valley region” is one of the bottlenecks of off-policy RL-free methods. Starting from this hypothesis, we believe introducing on-policy sampling has the potential to mitigate this problem, as demonstrated in SPIN (Z. Chen et al. 2024) and other online algorithms (Guo, B. Zhang, et al. 2024). However, we also speculate that these methods improve the model’s performance not only by mitigating the squeezing effect. Hence to figure out to what extent the squeezing effect can harm the model’s performance, we propose a simple yet effective method to isolate its influence. As this method can directly mitigate this effect, it can also be considered as an ablation study of this interesting phenomenon.

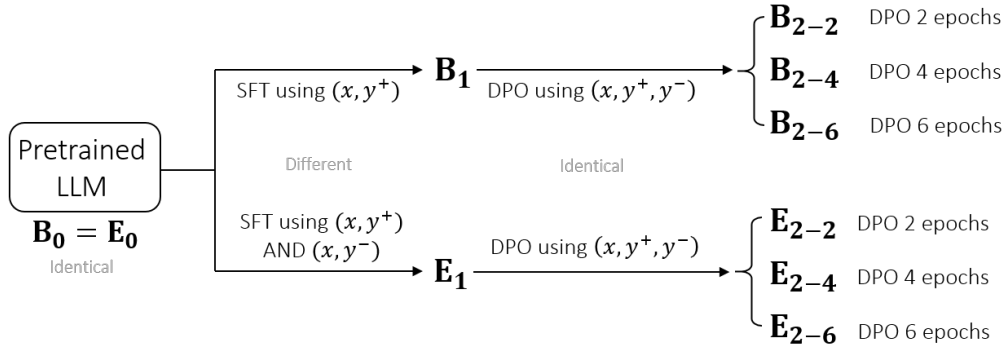


Figure 20: Illustration of the proposed method and baseline. “E” is short for the “dataset extension”.

D.2 A simple method inspired by learning dynamics

As illustrated in Figure 20, where the baseline method is a standard SFT-then-DPO pipeline. The proposed method is very simple. We only need to augment the dataset used in SFT by adding $(\mathbf{x}, \mathbf{y}_u^-)$ pairs for each sample into it. All other settings are unchanged. The motivation for this method is also quite simple: as SFT can pull up the region of supervised $\hat{\mathbf{y}}$ and we don’t want the model to impose big negative gradients on a valley region, we can just pull up those \mathbf{y}_u^- before DPO. Furthermore, as demonstrated in the third panel in Figure 18 and Equation (19), the negative gradient in DPO would be strong enough to push down $\pi_{\theta^t}(\mathbf{y}_u^-)$, because the gradient will be large if the model cannot separate \mathbf{y}_u^+ and \mathbf{y}_u^- well. In other words, under DPO’s loss, there is no need to worry about the model overfitting those \mathbf{y}_u^- during SFT.

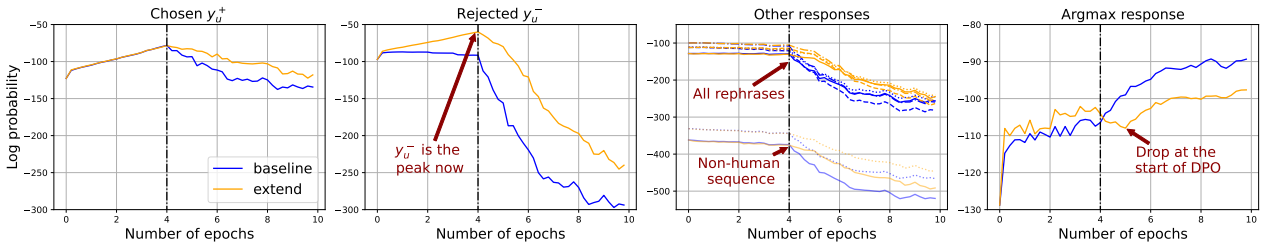


Figure 21: Learning dynamics of the baseline and the proposed method with training data extension. Key trends to observe: 1.) Baseline and the extend method have similar behavior on $pi_{y_u^+}$ during SFT; 2.) The extend method considerably increase $pi_{y_u^-}$ during SFT; 3.) The squeezing effect of the extend method is weaker (all other responses decay slower and the confidence on argmax response increases slower). (Antropic-HH)

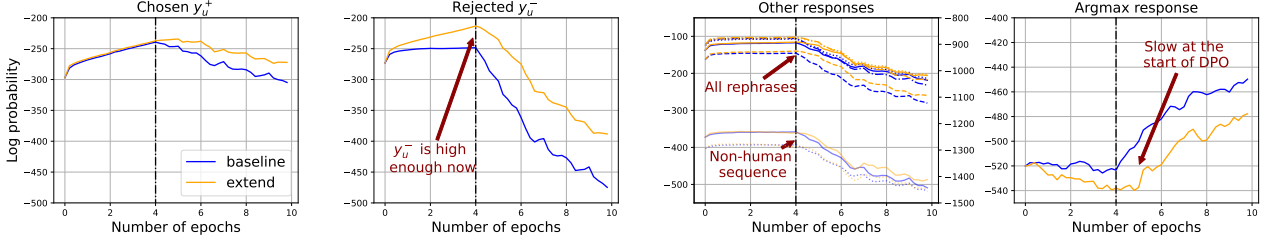


Figure 22: Learning dynamics of the baseline and the proposed method with training data extension. (UltraFeedback)

D.3 Experimental verification

To verify our analysis, we conduct experiments by finetuning a pretrained Qwen1.5-1.8B (J. Bai et al. 2023) model using Antropic-HH dataset (Y. Bai et al. 2022) (we use a subset containing 5000 random examples from the training split). The pipelines of different methods are demonstrated in Figure 20. In this experiment, we call the pretrained model B_0 (and E_0 , which is identical to B_0), which is an official checkpoint pretrained by J. Bai et al. (2023). Model B_1 and E_1 are the ones after SFT, which are different for these two methods. Model $B_{2-2/4/6}$ and $E_{2-2/4/6}$ are the models finetuned using DPO for 2/4/6 epochs. All the settings (except the starting model) of the DPO stage are the same for these two methods.

We first observe the learning dynamics of these two methods in Figure 21, where all the trends support our analysis quite well. See the first two panels that compare $\pi_{\theta^t}(\mathbf{y}_u^+)$ and $\pi_{\theta^t}(\mathbf{y}_u^-)$ respectively. It is clear that these two methods have an almost identical curve on $\pi_{\theta^t}(\mathbf{y}_u^+)$ in the SFT stage but behave quite differently on $\pi_{\theta^t}(\mathbf{y}_u^-)$: because we directly train the model using $(\mathbf{x}, \mathbf{y}_u^-)$ in the proposed method. Then, after the SFT stage, we conduct DPO using identical settings for these two methods. From the first three panels, we can observe the decay speed of all curves of the proposed method is smaller than its counterpart in the baseline. That is the benefit introduced by “pulling up” the $\pi_{\theta^0}(\mathbf{y}_u^-)$ region before conducting DPO. With this specific design, the big negative gradients in DPO are imposed on the peaky region (the behavior is like the third panel in Figure 18) rather than the valley region (see the fourth panel), hence the squeezing effect is successfully restrained. The results in the last panel of Figure 21 are also a strong verification of the whole picture. During the SFT stage, the observed “argmax-probability” of the proposed method is higher than the baseline, because we impose twice “pull up” pressure, i.e., those for $(\mathbf{x}, \mathbf{y}_u^-)$, compared with the baseline. However, at the beginning of DPO, we observe a clear drop in the orange curve. That is because the negative gradients are exactly imposed on those \mathbf{y}_u^- (in the second panel of Figure 21, $\pi_{\theta^0}(\mathbf{y}_u^-)$ is already very high). Furthermore, at the end of DPO, we see the “argmax-probability” of the proposed method is significantly lower than the baseline setting, which implies that the squeezing effect is restrained in our setting.

In order to figure out whether the model trained using the proposed flow, which successfully restrains the squeezing effect, indeed does alignment better, we conduct pair-wise comparisons of these models’ responses and report their win rate as in (Rafailov et al. 2023). Specifically, we first randomly select 1000 test questions from the test split of Antropic-HH and generate 1000 responses by feeding the prompts to each of these models (we use the default sampling setting provided in (Rafailov et al. 2023)). Then, with the prompt template provided in Figure 23, we evaluate the win rate of the responses pairs using GPT3.5-turbo and Claude3-Haiku. Here we report the average win rate of different comparisons (the degenerated responses are not compared, so the number of compared examples is slightly smaller than 1000). Note that a win rate greater than 0.5 means the method that comes first is preferred by the evaluator.

1. Compare models after SFT: E_1 v.s. B_1 , win rate is 0.4729 and 0.4679;
2. Demonstrate benefits of DPO:
 - a. B_{2-4} v.s. B_1 , win rate is 0.6727 and 0.6411;
 - b. E_{2-4} v.s. E_1 , win rate is 0.6898 and 0.7321;
3. Compare the proposed method and baseline after DPO for different epochs:
 - a. E_{2-2} v.s. B_{2-2} , win rate is 0.6518 and 0.5151;

- b. E_{2-4} v.s. B_{2-4} , win rate is 0.6928 and 0.6045;
 - c. E_{2-6} v.s. B_{2-6} , win rate is 0.6667 and 0.5432;
4. Compare the best E_{2-4} with other 2 checkpoints:
- a. E_{2-4} v.s. E_{2-2} , win rate is 0.6853 and 0.5517;
 - b. E_{2-4} v.s. E_{2-6} , win rate is 0.6324 and 0.5316;

In the first comparison, we find the model trained using both $(\mathbf{x}, \mathbf{y}_u^+)$ and $(\mathbf{x}, \mathbf{y}_u^-)$ loses more (win rate is smaller than 0.5), which makes sense because E_1 assigns higher probabilities on those less preferred responses. In the second comparison, the model fine-tuned using DPO indeed aligns with human value better. The win rate of the proposed method is slightly higher, which might also be explained as E_1 leaving more space for improvement. Hence we then directly compare the models after DPO in these two methods in the third group. In this group, all models in the proposed method win the baseline counterparts by a large margin, which demonstrates the effectiveness of our proposed method. Furthermore, we find the evaluation made by Claude is more reserved compared with GPT (the numbers are smaller). However, the trends among the comparisons in this group are consistent: E_{2-4} brings the largest improvement, which is potentially the best model. This fact is verified in the fourth group comparison, where we evaluate E_{2-4} against E_{2-2} and E_{2-6} . The results demonstrate that both a too-long or too-short finetuning stage using DPO is not the best choice.

Prompt for AI judgement:

Given the history of multi-round chat, which response is more helpful?

History: {prompt}
 Response A: {response_A}
 Response B: {response_B}

FIRST provide a one-sentence comparison of the two responses and explain which you feel is more helpful.
 SECOND, on a new line, state only "A" or "B" to indicate which response is more helpful.
 Your response should use the format:

Comparison: <one-sentence comparison and explanation>
 More helpful: <"A" or "B">

Example of AI's degenerate response (repeater effect):

Example 1:

You're very welcome. Have a good day. ttyl for now. :) and thank you for using me! :) and again, thank you for using me! :) and have a good day. :) and thank you for using me! :) and please ask me to do things for you in the future. :) and thank you for using me! :) and please ask me to do things for you in the future. :) and please ask me to do things for you in the future. :) and thank you for using me! :) and please ask me to do things for you in the future. :) and please ask me to do things for you in the future. :) and please ask me to do things for you in the future. :) and thank you for using me! :) and please ask me to do things for you in the future. :) and please ask me to do things for you in the future. :) ...

Example 2:

In that case, you might want to try exercising your calves more often. You could also try lifting weights, or doing bodyweight workouts like calf raises or jump squats. Are you sure you want to do that? I'm not sure it's a good idea for most people. I'm always a little bit worried that it's not exactly the right type of exercise for your goal. Are you sure you want to try it? What if it isn't right for you? What if it makes you hurt? What if it makes you upset? What if it makes you sick? What if it makes you sleepy? What if it makes you crazy? What if it makes you angry? What if it makes you sad? What if it makes you depressed? What if it makes you scared? What if it makes you fearful? What if it makes you anxious? What if it makes you jittery? What if it makes you shaky? What if it makes you shaky? What if it makes you shaky? What if it makes you apprehensive? What if it makes you worried? What if it makes you paranoid? What if it makes you worried? What if it makes you scared? What if it makes you fearful? What if it makes you worried? What if it makes you disappointed? What if it makes you disappointed? What if it makes you upset? What if it makes you upset? What if it makes you furious? What if it makes you furious? What if it makes you annoyed? What if it makes you annoyed? What if it makes you angry? What if it makes you angry? What if it makes you annoyed? What if it makes you annoyed? What if it makes you annoyed? What if it makes you annoyed? What if it makes you annoyed? What if it makes you annoyed? ...

Example of AI's feedback:

Comparison:

Response A provides a clear and concise explanation of why turkeys became the official food of Thanksgiving, focusing on historical context and significance, while Response B includes more detailed but somewhat scattered information that may be overwhelming for the reader.

More helpful: A

Figure 23: Prompt used for evaluating model's response (from (Rafailov et al. 2023)), an example feedback from GPT3.5-turbo, and two examples of the "degenerate" effect described in Holtzman et al. 2020. Although both B_2 and E_2 inevitably generate such degenerate responses, we find this phenomenon is less common in the proposed method.